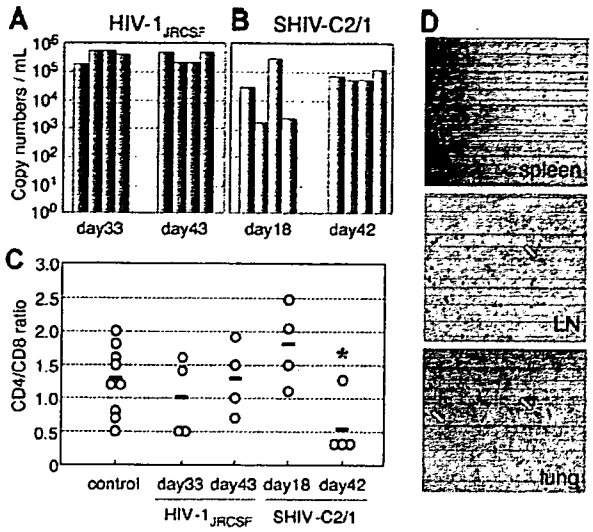

Figure 4. The numbers of RNA viral copies in plasma, CD4+/CD8+ T-cell ratios in the spleen, and p24 detection in the immunohistochemistry of HIV/SHIV-infected mice. (A) Viral copy numbers of 8 mice inoculated with a high infectious dose of HIV-1_{JRCSF} (65 000 $TCID_{50}$) and killed on days 33 and 43 after inoculation. (B) Viral copy numbers of 8 mice inoculated with a high infectious dose of SHIV-C2/1 (50 000 $TCID_{50}$) and killed on days 18 and 42 after inoculation. Note that all the mice showed high levels of viremia that lasted more than 40 days after inoculation. (C) CD4/CD8 cell ratios in the spleens of 16 infected mice and 9 uninfected control mice. Control mice were not inoculated with HIV/SHIV and were killed on days 105 to 166 after stem cell transplantation. There was no significant rapid loss of $CD4^+$ cells in HIV-1_{JRCSF}–infected mice, while a decline of the CD4/CD8 ratio was detected in SHIV-C2/1–infected mice on day 42 after infection compared with uninfected control mice (*$P < .05$). The short bars indicate the means of each group. (D) $P24^+$ cells are clearly observed in the spleen, LNs, and lungs. Arrow indicates p24 positive for macrophage-like cells. Original magnification, ×100.

dose of HIV-1_{JRCSF} and 2 of the 3 mice given a low dose of HIV-1_{MNp} were successfully infected (Table 1), suggesting that each dose represents an approximately 50% infectious dose of HIV for hNOG mice. High HIV-DNA copy numbers were mainly detected in the spleen and BM of the HIV-1_{JRCSF} –infected mice, and in the thymus and spleen of the HIV-1_{MNp}–infected mice, while their BM showed lower copy numbers (Table 1).

Generation of HIV-specific antibodies in hNOG mice at a high multiplicity of infection

We then tested for generation of human antibodies against HIV-1 from these 14 mice by HIV antigen-specific ELISA. The sera of mice no. 136-3 and no. 157-3 infected with HIV-1_{JRCSF} and HIV-1_{MNp}, respectively, showed significant levels of human antibodies specific for HIV-1_{IIIB}-Env gp120 (Figure 5A), HIV-1_{MN}-Env gp120 (Figure 5B), and HIV-1_{IIIB}-Gag p24 (Figure 5C). In addition, no. 157-4 sera from an HIV-1_{MNp}–infected animal was also weakly positive for their Env and Gag antigens. These animals showed intense plasma viral loads and enhanced proviral DNA copies in the spleen, BM, and thymus (Table 1), suggesting that hNOG mice inoculated with high doses of HIV and showing high rates of viral infection develop HIV-1–specific humoral immune responses that are analogous to those seen in human anti-HIV B-cell responses.

Discussion

Current small-animal models fall short of accurately mirroring human HIV-1 infection and thus have limited usefulness in analyzing the natural course of its progression to the disease state and in developing antiviral countermeasures. Although successful HIV-1 infections in immunodeficiency mice humanized with PBMCs have been reported,[12,13,21] transplanted human cells are soon depleted and do not elicit virus-specific immune responses, shedding little light on pathogenesis and vaccine development. By using NOG mice that received hematopoietic stem cell transplants showing high rates of viral infection, we demonstrated HIV-specific antibody responses and viral infection parameters, including the following: (1) similar levels of susceptibility to both R5- and X4-tropic HIV-1; (2) high levels of viremia stably observed over 40 days; (3) immunohistochemical detection of infected cells in various organs; and (4) a distinct tissue distribution for R5- versus X4-tropic HIV-1s.

Among $CD4^+$ T cells, CXCR4 antigen is primarily expressed on naive and CCR5 on activated or memory cells.[26] hu-PBL-SCID mice become susceptible to R5-tropic HIV-1 strains,[27] since T cells

Table 1. Comparison of viral RNA copies in plasma and HIV-DNA copies in the spleen, BM, and thymus from hNOG mice receiving low- and high-dose viral inoculations

Mouse ID no.	HIV strain	$TCID_{50}$	Time after inoculation, d	RNA viral copies/mL	CD4/CD8 ratio	HIV-DNA copies/10^6 human cells		
						Spleen	BM	Thymus
Low-dose viral inoculation group								
113-1	HIV-1_{JRCSF}	200	18	6 240	1.8	34 177	11 785	3 495
112-2	HIV-1_{JRCSF}	200	18	<500	1.2	< 100	< 100	< 100
113-2	HIV-1_{JRCSF}	200	40	6 177	1.6	25 855	27 920	3 473
112-3	HIV-1_{JRCSF}	200	40	<500	0.9	< 100	< 100	<100
112-4	HIV-1_{MNp}	180	18	72 477	1.3	18 873	100	ND
113-4	HIV-1_{MNp}	180	40	70 667	0.3	4 947	653	32 163
112-1	HIV-1_{MNp}	180	40	<500	0.9	< 100	< 100	< 100
High-dose viral inoculation group								
136-3	HIV-1_{JRCSF}	65 000	25	252 381	0.8	958 871	1 797 600	232 155
136-2	HIV-1_{JRCSF}	65 000	29	50 167	0.7	41 172	54 521	8 600
141-1	HIV-1_{JRCSF}	65 000	30	67 667	2.2	27 735	52 430	429
161-3	HIV-1_{JRCSF}	65 000	30	13 847	0.9	104 466	14 653	111 080
157-3	HIV-1_{MNp}	20 000	31	1 253 925	0.5	41 053	56 802	976 556
157-4	HIV-1_{MNp}	20 000	31	147 973	0.6	3 634	262	40 796
161-6	HIV-1_{MNp}	20 000	31	108 073	1.7	4 991	< 100	3 673

Seven mice inoculated with a low infectious dose of HIV-1_{JRCSF} (200 $TCID_{50}$) or HIV-1_{MNp} (180 $TCID_{50}$), and 7 mice receiving a high infectious dose of HIV-1_{JRCSF} (65 000 $TCID_{50}$) or HIV-1_{MNp} (20 000 $TCID_{50}$) were listed.
ND indicates not done.

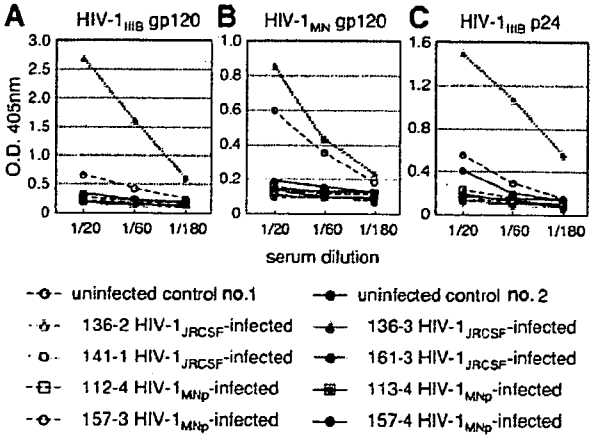

Figure 5. Detection of anti–HIV-1 antibodies from the plasma of HIV-1–infected mice. An ELISA assay was conducted by using plasma from 14 mice inoculated with either HIV-1_{JRCSF} or HIV-1_{MNp}, and from 2 uninfected control mice. Representatives (n = 8) of the 14 HIV-1–inoculated mice, and the 2 uninfected mice, are shown in the panels. Measurements of specific human antibodies for HIV-1_{IIIB} gp120 (A), HIV-1_{MN} gp120 (B), and HIV-1_{IIIB} p24 antigens (C) were shown. Results are expressed as the means from triplicate assays in 3 different experiments.

are initially activated in the xenogenic environment and then become anergic.[14] In contrast, SCID-hu (Thy/Liv) mice are more susceptible to X4 than to R5 strains[6] because HIV-1 infection is restricted mainly to the engrafted thymus that is primarily comprised of immature T cells, suggesting that this model may not be practical overt HIV infection. Our study represents the first attempt to infect NOG mice that received transplants of human hematopoietic stem cells with HIV-1. Very similar infection rates were seen for both R5 and X4 strains in the mouse model. Flow cytometry revealed both $CXCR4^+CD4^+$ and $CCR5^+CD4^+$ cells in PB, the spleen, and BM, but only CXCR4 on thymic $CD4^+$ T cells. It also showed the scattering of human macrophages, known to be susceptible to R5-tropic HIV-1 strains[28,29] and the source of HIV-1,[23,30-32] throughout various organs. $p24^+$ macrophage-like cells were detected in these organs after R5-tropic HIV-1_{JRCSF} infection. These data may help explain the susceptibility of hNOG mice to both R5- and X4-tropic HIV strains and also shed light on the active replenishment of these target cells in mice.

SCID mouse systems have been actively used in the evaluation of anti–HIV-1 drugs.[9,11,21] In most cases, HIV-1 detection levels reach a peak within a month after inoculation and level off, accompanied by $CD4^+$ T-cell depletion.[3,12,13] Although suitable for short-term experiments, it is also true that these models require large numbers of mice because of large variations in infection efficiency. In contrast, very stable infections were noted in our hNOG mice that were inoculated with a high dose of HIVs. They did not show rapid CD4/CD8 decrease in spite of high levels of viremia persisting for more than 40 days. Efficient hematopoiesis and thymopoiesis of human cells probably compensated for the loss of $CD4^+$ T cells, allowing for persistent infection. This capacity of the hNOG mouse system makes it attractive as a model for the long-term evaluation of anti–HIV-1 drugs. In addition to destroying mature blood cells, altered hematopoiesis in BM and the thymus has also been reported to be responsible for immunodeficiency in patients with AIDS.[33,34] To study hematopoietic abnormalities in HIV-1 infection, both SCID-hu (Thy/Liv) mice[8,35,36] and SIV- or SHIV-infected macaque models[20,37-39] have been used. The current hNOG mouse system, in which human cells are efficiently reproduced from stem cells and then settled into hematopoietic organs, offers a promising model for the study of events that occur after infection not only with R5-tropic HIV-1 but also with X4-tropic HIV-1. Indeed, the BM of hNOG mice infected with R5-tropic HIV-1 exhibited exceptionally elevated levels of HIV-DNA copies. On the other hand, the thymus of X4-tropic HIV-1_{MNp}–infected hNOG mice yielded large numbers of HIV-DNA copies, which seemed to correlate with the predominant expression of CXCR4 on the thymocytes. Thus, further observation is essential to address whether AIDS symptoms such as considerable $CD4^+$ T-cell depletion and hematopoietic abnormalities eventually occur in these mice.

It is noteworthy that human antibodies against both HIV-1 Env gp120 and Gag p24 antigens were detected in mice no. 136-3, no. 157-3, and no. 157-4 after exposure to high titers of HIV-1, suggesting that hNOG mice have the ability to respond to HIV-1 antigens. This encourages us to develop antibody-based HIV vaccine candidates, although additional modifications are required for the stable induction of immune responses. Importantly, since the seroconverted mice showed high viremia and high numbers of proviral DNA copies in the spleen, BM, and thymus, abundant viral production may stimulate human B-cell responses against HIV-1 and generate specific antibodies. These mice showed little or no detectable human IgG against HIV-1, as determined by Western blot analysis (data not shown), suggesting that very low levels of class-switching occurred in these mice, though further study is required.

In addition to the humoral immune responses, the induction of primary T-cell responses is critical for the study of HIV-specific immune responses and pathogenesis, as well as for vaccine development. Although we did not demonstrate the T-cell ability to respond to virus antigens, human T cells from the spleen proliferated when stimulated with anti–human CD3 antibodies (data not shown), indicating that the human T cells in the NOG mice that received transplants of hematopoietic stem cells are capable of responding to T-cell receptor–mediated signals and are expected to be able to elicit primary antigen-specific immune responses against foreign antigens. To address whether the specific T-cell responses may be induced will be one of the important studies.

In conclusion, the NOG mice that received transplants of human hematopoietic stem cells successfully achieved systemic and persistent infection with both R5-tropic and X4-tropic HIV-1, and generated humoral immune responses against HIV-1. These capacities of the hNOG mouse model may be very attractive for the study of HIV pathogenesis and humoral immune responses induced by HIV vaccine candidates.

Acknowledgments

We thank Yuetsu Tanaka of the University of Ryukyus, Tetsutaro Sata of NIID, and Shuzo Matsushita of Kumamoto University for their kind provision of mAbs to HIV-1, as well as Yukoku Tamaoka of Saiseikai Central Hospital, Toshio Akashi of Kumakiri Obstetric and Gynecologic Clinic, and Hideo Mugishima of Nihon University School of Medicine for their provision of umbilical cord blood. We also would like to express our gratitude to Ken Watanabe and Hideko Ogata of Tokyo Medical and Dental University for their skillful technical support.

This work was supported by grants from Research on Health Sciences focusing on Drug Innovation, the Japan Health Sciences Foundation.

Authorship

Contributions: S.W., K.T., N.S., M.H., and N.Y. designed the study; S.W., K.T., S.O., S.H., M.Y., Y.S., M.Z.D., and Z.Y. carried out the research; M.I. contributed live mice; S.W., K.T., and T.M. analyzed the data; N.S., M.H., and N.Y. controlled the data; S.W. wrote the paper; and all authors checked the final version of the manuscript.

Conflict-of-interest statement: The authors declare no competing financial interests.

Correspondence: Naoki Yamamoto, AIDS Research Center, National Institute of Infectious Diseases, 1-23-1 Toyama, Shinjuku-ku, Tokyo 162-8640, Japan; e-mail: nyama@nih.go.jp; Mitsuo Honda, AIDS Research Center, National Institute of Infectious Diseases, 1-23-1 Toyama, Shinjuku-ku, Tokyo 162-8640, Japan; e-mail: mhonda@nih.go.jp; and Norio Shimizu, Department of Virology, Division of Medical Science, Medical Research Institute, Tokyo Medical and Dental University, 1-5-45 Yushima, Bunkyo-ku, Tokyo 113-8519, Japan; e-mail: nshivir@tmd.ac.jp.

References

1. Letvin NL, Barouch DH, Montefiori DC. Prospects for vaccine protection against HIV-1 infection and AIDS. Annu Rev Immunol. 2002;20:73-99.
2. Namikawa R, Kaneshima H, Lieberman M, Weissman IL, McCune JM. Infection of the SCID-hu mouse by HIV-1. Science. 1988;242: 1684-1686.
3. Bonyhadi ML, Rabin L, Salimi S, et al. HIV induces thymus depletion in vivo. Nature. 1993; 363:728-732.
4. Aldrovandi GM, Feuer G, Gao L, et al. The SCID-hu mouse as a model for HIV-1 infection. Nature. 1993;363:732-736.
5. Su L, Kaneshima H, Bonyhadi M, et al. HIV-1-induced thymocyte depletion is associated with indirect cytopathogenicity and infection of progenitor cells in vivo. Immunity. 1995;2:25-36.
6. Kaneshima H, Su L, Bonyhadi ML, Connor RI, Ho DD, McCune JM. Rapid-high, syncytium-inducing isolates of human immunodeficiency virus type 1 induce cytopathicity in the human thymus of the SCID-hu mouse. J Virol. 1994;68:8188-8192.
7. Jenkins M, Hanley MB, Moreno MB, Wieder E, McCune JM. Human immunodeficiency virus-1 infection interrupts thymopoiesis and multilineage hematopoiesis in vivo. Blood. 1998;91:2672-2678.
8. Koka PS, Fraser JK, Bryson Y, et al. Human immunodeficiency virus inhibits multilineage hematopoiesis in vivo. J Virol. 1998;72:5121-5127.
9. Mosier DE, Gulizia RJ, Baird SM, Wilson DB, Spector DH, Spector SA. Human immunodeficiency virus infection of human-PBL-SCID mice. Science. 1991;251:791-794.
10. Torbett BE, Picchio G, Mosier DE. hu-PBL-SCID mice: a model for human immune function, AIDS, and lymphomagenesis. Immunol Rev. 1991;124: 139-164.
11. Ruxrungtham K, Boone E, Ford H Jr, Driscoll JS, Davey RT Jr, Lane HC. Potent activity of 2'-beta-fluoro-2',3'-dideoxyadenosine against human immunodeficiency virus type 1 infection in hu-PBL-SCID mice. Antimicrob Agents Chemother. 1996;40:2369-2374.
12. Mosier DE, Gulizia RJ, MacIsaac PD, Torbett BE, Levy JA. Rapid loss of CD4+ T cells in human-PBL-SCID mice by noncytopathic HIV isolates. Science. 1993;260:689-692.
13. Koyanagi Y, Tanaka Y, Kira J, et al. Primary human immunodeficiency virus type 1 viremia and central nervous system invasion in a novel hu-PBL-Immunodeficient mouse strain. J Virol. 1997; 71:2417-2424.
14. Tary-Lehmann M, Saxon A, Lehmann PV. The human immune system in hu-PBL-SCID mice. Immunol Today. 1995;16:529-533.
15. Ito M, Hiramatsu H, Kobayashi K, et al. NOD/SCID/gamma(c)(null) mouse: an excellent recipient mouse model for engraftment of human cells. Blood. 2002;100:3175-3182.
16. Yahata T, Ando K, Nakamura Y, et al. Functional human T lymphocyte development from cord blood CD34+ cells in nonobese diabetic/Shi-scid, IL-2 receptor gamma null mice. J Immunol. 2002; 169:204-209.
17. Hiramatsu H, Nishikomori R, Heike T, et al. Complete reconstitution of human lymphocytes from cord blood CD34+ cells using the NOD/SCID/gammacnull mice model. Blood. 2003;102:873-880.
18. Matsumura T, Kametani Y, Ando K, et al. Functional CD5+ B cells develop predominantly in the spleen of NOD/SCID/gammac(null) (NOG) mice transplanted either with human umbilical cord blood, bone marrow, or mobilized peripheral blood CD34+ cells. Exp Hematol. 2003;31:789-797.
19. Shinohara K, Sakai K, Ando S, et al. A highly pathogenic simian/human immunodeficiency virus with genetic changes in cynomolgus monkey. J Gen Virol. 1999;80:1231-1240.
20. Yamakami K, Honda M, Takei M, et al. Early bone marrow hematopoietic defect in simian/human immunodeficiency virus C2/1-infected macaques and relevance to advance of disease. J Virol. 2004;78:10906-10910.
21. Nakata H, Maeda K, Miyakawa T, et al. Potent anti-R5 human immunodeficiency virus type 1 effects of a CCR5 antagonist, AK602/ONO4128/GW873140, in a novel human peripheral blood mononuclear cell nonobese diabetic-SCID, interleukin-2 receptor gamma-chain-knocked-out AIDS mouse model. J Virol. 2005;79:2087-2096.
22. Heath SL, Tew JG, Tew JG, Szakal AK, Burton GF. Follicular dendritic cells and human immunodeficiency virus infectivity. Nature. 1995;377:740-744.
23. Orenstein JM, Fox C, Wahl SM. Macrophages as a source of HIV during opportunistic infections. Science. 1997;276:1857-1861.
24. van Kooyk Y, Geijtenbeek TB. A novel adhesion pathway that regulates dendritic cell trafficking and T cell interactions. Immunol Rev. 2002;186: 47-56.
25. Taylor JR Jr, Kimbrell KC, Scoggins R, Delaney M, Wu L, Camerini D. Expression and function of chemokine receptors on human thymocytes: implications for infection by human immunodeficiency virus type 1. J Virol. 2001;75:8752-8760.
26. Bleul CC, Wu L, Hoxie JA, Springer TA, Mackay CR. The HIV coreceptors CXCR4 and CCR5 are differentially expressed and regulated on human T lymphocytes. Proc Natl Acad Sci U S A. 1997; 94:1925-1930.
27. Fais S, Lapenta C, Santini SM, et al. Human immunodeficiency virus type 1 strains R5 and X4 induce different pathogenic effects in hu-PBL-SCID mice, depending on the state of activation/differentiation of human target cells at the time of primary infection. J Virol. 1999;73:6453-6459.
28. Gartner S, Markovits P, Markovitz DM, Kaplan MH, Gallo RC, Popovic M. The role of mononuclear phagocytes in HTLV-III/LAV infection. Science. 1986;233:215-219.
29. Koyanagi Y, Miles S, Mitsuyasu RT, Merrill JE, Vinters HV, Chen IS. Dual infection of the central nervous system by AIDS viruses with distinct cellular tropisms. Science. 1987;236:819-822.
30. Gendelman HE, Orenstein JM, Baca LM, et al. The macrophage in the persistence and pathogenesis of HIV infection. AIDS. 1989;3:475-495.
31. Embretson J, Zupancic M, Ribas JL, et al. Massive covert infection of helper T lymphocytes and macrophages by HIV during the incubation period of AIDS. Nature. 1993;362:359-362.
32. Igarashi T, Brown CR, Endo Y, et al. Macrophage are the principal reservoir and sustain high virus loads in rhesus macaques after the depletion of CD4+ T cells by a highly pathogenic simian immunodeficiency virus/HIV type 1 chimera (SHIV): implications for HIV-1 infections of humans. Proc Natl Acad Sci U S A. 2001;98:658-663.
33. Mir N, Costello C, Luckit J, Lindley R. HIV-disease and bone marrow changes: a study of 60 cases. Eur J Haematol. 1989;42:339-343.
34. Moses A, Nelson J, Bagby GC Jr. The influence of human immunodeficiency virus-1 on hematopoiesis. Blood. 1998;91:1479-1495.
35. Koka PS, Jamieson BD, Brooks DG, Zack JA. Human immunodeficiency virus type 1-induced hematopoietic inhibition is independent of productive infection of progenitor cells in vivo. J Virol. 1999;73:9089-9097.
36. Koka PS, Kitchen CM, Reddy ST. Targeting c-Mpl for revival of human immunodeficiency virus type 1-induced hematopoietic inhibition when CD34+ progenitor cells are re-engrafted into a fresh stromal microenvironment in vivo. J Virol. 2004;78: 11385-11392.
37. Hillyer CD, Lackey DA 3rd, Villinger F, Winton EF, McClure HM, Ansari AA. CD34+ and CFU-GM progenitors are significantly decreased in SIVsmm9 infected rhesus macaques with minimal evidence of direct viral infection by polymerase chain reaction. Am J Hematol. 1993;43:274-278.
38. Thiebot H, Louache F, Vaslin B, et al. Early and persistent bone marrow hematopoiesis defect in simian/human immunodeficiency virus-infected macaques despite efficient reduction of viremia by highly active antiretroviral therapy during primary infection. J Virol. 2001;75:11594-11602.
39. Thiebot H, Vaslin B, Derdouch S, et al. Impact of bone marrow hematopoiesis failure on T-cell generation during pathogenic simian immunodeficiency virus infection in macaques. Blood. 2005; 105:2403-2409.

Inhibiting lentiviral replication by HEXIM1, a cellular negative regulator of the CDK9/cyclin T complex

Saki Shimizu[a,b], Emiko Urano[a], Yuko Futahashi[a], Kosuke Miyauchi[a], Maya Isogai[a], Zene Matsuda[a], Kyoko Nohtomi[a], Toshinari Onogi[a], Yutaka Takebe[a], Naoki Yamamoto[a,b] and Jun Komano[a]

Objective: Tat-dependent transcriptional elongation is crucial for the replication of HIV-1 and depends on positive transcription elongation factor b complex (P-TEFb), composed of cyclin dependent kinase 9 (CDK9) and cyclin T. Hexamethylene bisacetamide-induced protein 1 (HEXIM1) inhibits P-TEFb in cooperation with 7SK RNA, but direct evidence that this inhibition limits the replication of HIV-1 has been lacking. In the present study we examined whether the expression of FLAG-tagged HEXIM1 (HEXIM1-f) affected lentiviral replication in human T cell lines.

Methods: HEXIM1-f was introduced to five human T cell lines, relevant host for HIV-1, by murine leukemia virus vector and cells expressing HEXIM1-f were collected by fluorescence activated cell sorter. The lentiviral replication kinetics in HEXIM1-f-expressing cells was compared with that in green fluorescent protein (GFP)-expressing cells.

Results: HIV-1 and simian immunodeficiency virus replicated less efficiently in HEXIM1-f-expressing cells than in GFP-expressing cells of the five T cell lines tested. The viral revertants were not immediately selected in culture. In contrast, the replication of vaccinia virus, adenovirus, and herpes simplex virus type 1 was not limited. The quantitative PCR analyses revealed that the early phase of viral life cycle was not blocked by HEXIM1. On the other hand, *Tat*-dependent transcription in HEXIM1-f-expressing cells was substantially repressed as compared with that in GFP-expressing cells.

Conclusion: These data indicate that HEXIM1 is a host factor that negatively regulates lentiviral replication specifically. Elucidating the regulatory mechanism of HEXIM1 might lead to ways to control lentiviral replication.

AIDS 2007, **21**:575–582

Keywords: CDK9, cyclin T, HEXIM1, lentivirus, *tat*

Introduction

Activation of transcription elongation requires the positive transcription elongation factor b complex (P-TEFb) composed of cyclin dependent kinase 9 (CDK9) and cyclin T1, T2, or K [1]. P-TEFb is essential for efficient transcriptional elongation from the promoter of human immunodeficiency virus type 1 (HIV-1), the long terminal repeat (LTR) (reviewed in [2,3]). The functional interaction between P-TEFb and the viral protein Tat has been well studied. Immediately after viral transcription starts at the LTR of the integrated proviral genome, the nascent viral transcript forms a three-dimensional structure called TAR. In the presence of P-TEFb, Tat binds to TAR. Through the Tat–TAR interaction, Tat activates P-TEFb and therefore assures the efficient

From the [a]AIDS Research Center, National Institute of Infectious Diseases, Tokyo, and the [b]Department of Molecular Virology, Tokyo Medical and Dental University, Tokyo, Japan.

Correspondence to Jun Komano, AIDS Research Center, National Institute of Infectious Diseases, 1-23-1 Toyama, Shinjuku, Tokyo 162-8640, Japan.

E-mail: ajkomano@nih.go.jp

Received: 9 July 2006; revised: 25 October 2006; accepted: 13 November 2006.

ISSN 0269-9370 © 2007 Lippincott Williams & Wilkins

completion of viral gene transcription and the propagation of HIV-1.

Recently, the regulatory mechanisms of P-TEFb function have been elucidated. In 2001, the interaction of P-TEFb with 7SK RNA was found to be necessary to inactivate the kinase activity of CDK9 within P-TEFb [4–6]. However, the binding of 7SK RNA alone is not sufficient to inactivate P-TEFb. More recently, Yik *et al.* demonstrated that the inactivation of P-TEFb requires hexamethylene bisacetamide-induced protein 1 (HEXIM1; synonyms CLP1, MAQ1, and HIS1) [7–9]. The inactivation of P-TEFb by the HEXIM1-7SK RNA complex appears to regulate the transcriptional elongation of cellular genes.

The HEXIM1-7SK RNA complex has been shown to physically compete with Tat for binding to P-TEFb [10]. In agreement with this finding, HEXIM1 was shown to inhibit Tat-dependent transcription from the HIV-1 LTR in transient transfection assays [8,11,12]. However, no data demonstrating that HEXIM1 is able to limit HIV-1 replication has been provided. Here we provide direct experimental evidence that the constitutive expression of HEXIM1 specifically limits lentiviral replication.

Methods

Plasmids

The FLAG-tagged HEXIM1 expression constructs were generated by reverse-transcription PCR using RNA isolated from CEM cells as templates. The primers used were 5′-CACCTCGAGCCACCATGGACTACAAAGACGATGACGACAAGGCCGAGCCATTCTTGTC-3′ and 5′-CAATTGCTAGTCTCCAAACTTGGAAAGCGGCGC-3′′ for amino terminus FLAG tagging, and 5′-CACCTCGAGCCACCATGGCCGAGCCATTCTTGTCAGAATATC-3′ and 5′-CAATTGCTAGTCGTCATCGTCTTTGTAGTCGTCTCCAAACTTGGAAAGCGGCGCTC-3′ for carboxy terminus FLAG tagging. The *Xho*I-*Mfe*I fragments of the PCR products were cloned into the *Xho*I-*Mfe*I sites of pCMMP IRES GFP, generating pCMMP f-HEXIM1 and pCMMP HEXIM1-f [13]. The cytomegalovirus (CMV) promoter-driven *gag-pol* expression vector psyn*gag-pol* has been previously described by Wagner *et al.* [14] and pLTR*gag-pol* was constructed by cloning the *Mlu*I-*Hin*dIII fragment encoding the LTR from pNL-luc [15] into the *Mlu*I-*Hin*dIII sites of psyn*gag-pol*. The tax expressing plasmid pCGtax and pHTLV LTR luciferase were kindly provided by Dr. Watanabe (Tokyo Medical Institute). The *tat*-expressing plasmid pSVtat was a generous gift from Dr. Freed (National Cancer Institute-Frederick, Frederick, Maryland, USA). The plasmid pLTR-luc has been described previously (Miyauchi *et al.*, *Antiviral Chemistry and Chemotherapy*, in press). The following plasmids have been described previously by Komano *et al.* [13]: pVSV-G, pMD*gag-pol*, pTM3Luci, phRL-CMV and pSIVmac239ΔnefLuc.

Cells and transfection

All the mammalian cells were maintained in RPMI 1640 (Sigma, St Louis, Missouri, USA) supplemented with 10% fetal bovine serum (Japan Bioserum, Tokyo, Japan), penicillin and streptomycin (Invitrogen, Tokyo, Japan). Cells were incubated at 37°C in a humidified 5% CO_2 atmosphere. Cells were transfected using Lipofectamine 2000 according to the manufacturer's protocol (Invitrogen).

Western blotting

Cells were lysed with sample buffer, sonicated, and boiled for 5 min. Samples were separated on 8% sodium dodecyl sulfate-polyacrylamide gel electrophoresis gels and transferred to polyvinylidene difluoride membranes (Millipore, Billerica, Massachusetts, USA) for western blotting according to standard techniques. Membranes were blocked with Tris-buffered saline containing 0.05% Tween-20 (TBS-T) containing 5% (w/v) non-fat skim milk (Yuki-Jirushi, Tokyo, Japan) for 1 h at room temperature and incubated with primary antibodies including the M2 anti-FLAG epitope monoclonal antibody (Sigma), an anti-actin monoclonal antibody (MAB1501R; Chemicon/Millipore, Billerica, Massachusetts, USA), an anti-cyclin T1 rabbit polyclonal antibody (H-245; Santa Cruz Biotechnology, Santa Cruz, California, USA), an anti-cyclin T2a/b goat polyclonal antibody (A-20; Santa Cruz), an anti-p24 monoclonal antibody (183-H12-5C; NIH AIDS Research and Reference Reagent Program), an anti-HIS1 chicken polyclonal antibody (N-150; GenWay, San Diego, California, USA), and an anti-Bip/GRP78 monoclonal antibody (clone 40; BD Biosciences/Transduction Laboratories, San Jose, California, USA) for 1 h at room temperature. Membranes were washed with TBS-T and incubated with appropriate second antibodies including biotinylated anti-goat (GE Healthcare Bio-Sciences, Piscataway, New Jersey, USA) or anti-chicken IgY (Promega, Madison, Wisconsin, USA), and EnVision+ (Dako, Glostrup, Denmark) for 1 h at room temperature. For a tertiary probe, we used horseradish peroxidase (HRP)-streptavidine (GE Healthcare) if necessary. Signals were visualized with an LAS3000 imager (Fujifilm, Tokyo, Japan) after treating the membranes with the Lumi-Light Western Blotting Substrate (Roche Diagnostics GmbH, Mannheim, Germany).

Reporter assay

Luciferase activity was measured 48 h after transfection or infection using a DualGlo assay kit (Promega) according to the manufacturer's protocol. The beta-galactosidase activity was measured using a LumiGal assay kit (BD Biosciences/Clontech, San Jose, California, USA) according to the manufacturer's protocol. The

chemiluminescence was detected with a Veritas luminometer (Promega).

Monitoring viral replication

To monitor HIV-1 replication, the culture supernantants were subjected to either a reverse transcriptase assay [16] or an enzyme-linked immunosorbent assay (ELISA) to detect p24 antigens using a Retro TEK p24 antigen ELISA kit according to the manufacturer's protocol (Zepto Metrix, Buffalo, New York, USA). For simian immunodeficiency virus (SIV) a p27 antigen ELISA kit was used according to the manufacturer's protocol (Zepto Metrix). The signals were measured with a Multiskan Ex microplate photometer (ThermoLabsystems, Helsinki, Finland). For vaccinia virus, adenovirus, and herpes simplex virus (HSV)-1, the activity of reporter genes was measured as previously described [13].

Generating viruses

To produce HIV-1 and SIV, 293T cells were transfected with plasmids encoding proviral DNA of HIV-1 (pHXB2) or pSIVmac239ΔnefLuc and culture supernatants containing viruses were collected at 48 h post-transfection. Murine leukemia virus (MLV) and lentiviral vectors pseudotyped with VSV-G were produced as described previously by cotransfecting 293T cells with either the pNL-Luc and pVSV-G vectors or the pMD*gag-pol*, pVSV-G, and pCMMP vectors [13]. Green fluorescent cells were sorted by fluorescence activated cell sorter (FACS) Aria (Becton Dickinson, San Jose, California, USA).

Reverse transcriptase-polymerase chain reaction

Total RNA was isolated with an RNeasy kit (Qiagen GmbH, Hilden, Germany) according to the manufacturer's instruction. The reverse transcriptase (RT)-polymerase chain reaction (PCR) assay was performed with a One Step RNA PCR Kit (Takara, Otsu, Japan), imaged by a Typhoon scanner 9400 (GE Healthcare), and quantified with Image Quant software (GE Healthcare). For the amplification of endogenous HEXIM1, the forward primer 5′-ACCACACGGAGAGCCTGCAGAAC-3′ and the reverse primer 5′-TAGCTAAATTTACGAAACCAAAGCC-3′ were used. For the amplification of HEXIM1-f, the forward primer 5′-GTACCTGGAACTGGAGAAGTGCCC-3′ and the reverse primer 5′-CAATTGCTAGTCGTCATCGTCTTTGTAGTC-3′ were used. For cyclophilin A, the forward primer 5′-CACCGCCACCATGGTCAACCCCACCGTGTTCTTCGAC-3′ and the reverse primer 5′-CCCGGGCCTCGAGCTTTCGAGTTGTCCACAGTCAGCAATGG-3′ were used.

Quantitative real time polymerase chain reaction

The real time PCR reaction was performed in a DNA Engine Opticon 2 Continuous Fluorescence Detection System (Bio-Rad, Hercules, California, USA). The cellular genomic DNA and total RNA were extracted 48 h post-infection with a DNeasy kit (Qiagen) and RNeasy kit (Qiagen), respectively, according to the manufacturer's instruction. For the reagents, we used QuantiTect SYBR Green PCR and RT-PCR Kits (Qiagen). To estimate the amount of integrated HIV-1 DNA, Alu-LTR PCR was performed according to the method described previously using the following primers: for the first PCR, 5′-AACTAGGGAACCCACTGCTTAAG-3′ and 5′-TGCTGGGATTACAGGCGTGAG-3′, and for the second PCR, 5′-AACTAGGGAACCCACTGCTTAAG-3′ and 5′-CTGCTAGAGATTTTCCACACTGAC-3′ [17]. The beta-globin primers have been described previously [18]. To estimate the amount of HIV-1 RNA, the second PCR primers for the Alu-LTR PCR were used. The primers for cyclophilin A are described above.

Results and discussion

The HEXIM1 cDNA tagged with a FLAG epitope at either the amino terminus (f-HEXIM1) or the carboxy terminus (HEXIM1-f) was cloned in a mammalian expression plasmid (Fig. 1a). A luciferase assay revealed that the Tat-dependent enhancement of transcription from the HIV-1 LTR was reduced by co-transfecting HEXIM1-expressing plasmids, whereas neither Tat-independent basal transcription from the HIV-1 LTR nor CMV promoter-driven transcription was affected (Fig. 1b). An oncogenic retrovirus human T cell leukemia virus type 1 (HTLV-1) encodes for *tax*, a functional homologue of HIV-1's *tat*, that utilizes P-TEFb to enhance transcription from the LTR promoter [19]. However, *tax*-dependent enhancement of transcription was not affected by HEXIM1 in similar experimental conditions (Fig. 1c). To monitor the effect of HEXIM1 on HIV-1 replication, we introduced HEXIM1-expressing plasmids into HeLa-CD4 cells along with pNL4-3, which produces replication-competent HIV-1, and measured the RT activity in the culture supernatant 1 week post-transfection. Transfecting HEXIM1-expressing plasmids decreased the RT activity in a dose-dependent manner (Fig. 1d). Next, we asked whether the inhibition of viral replication was specific to HIV-1 by examining vaccinia virus, adenovirus, and HSV-1 replication. We found that the propagation of these three viruses was not inhibited by HEXIM1-f expression (Fig. 1e–g), suggesting that the inhibition of viral replication by HEXIM1 was HIV-1-specific.

To examine whether HEXIM1 negatively affects lentiviral replication in the physiologically relevant host, we isolated human T cell lines constitutively expressing HEXIM1-f. We cloned HEXIM1-f cDNA into a pCMMP (MLV retroviral vector plasmid (Fig. 2a). The plasmid encoded an internal ribosomal entry site (IRES)-mediated green fluorescent protein (GFP) expression cassette, so that MLV vector-infected cells

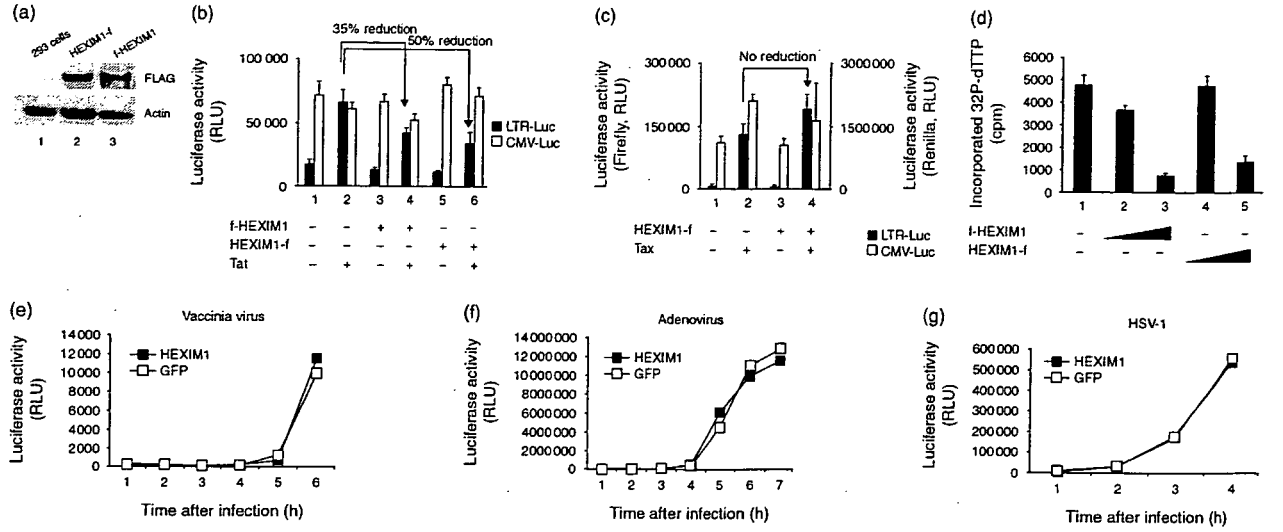

Fig. 1. Expression of hexamethylene bisacetamide-induced protein 1 (HEXIM1) specifically inhibits HIV-1 replication. (a) Detection of HEXIM1 cDNA tagged with a FLAG epitope at either the amino terminus (f-HEXIM1) or the carboxy terminus (HEXIM1-f) by western blot analysis in transiently transfected 293 cells (upper panel, approximately 65 kD). A western blot against actin is shown as a loading control (lower panel). (b) Expressing FLAG-tagged HEXIM1 decreased the luciferase activity driven by HIV-1 long terminal repeat (LTR) promoter in the presence of Tat (lanes 4 and 6, LTR-Luc, solid bars). However, FLAG-tagged HEXIM1 did not affect the expression of renilla luciferase from co-transfected plasmid driven by the cytomegalovirus (CMV) promoter (CMV-Luc, open bars). Representative data from three independent experiments done in triplicate are shown. Cells were transfected with 0.8 μg HEXIM1-expressing plasmid for the indicated lanes, 0.1 μg of pSV*tat* for the indicated lanes, and 0.1 μg of pLTR-Luc and 0.5 μg for phRL/CMV for all lanes. (c) Expressing FLAG-tagged HEXIM1 did not decrease the luciferase activity driven by HTLV-1 LTR promoter in the presence of Tax (lanes 2 and 4, LTR-Luc, solid bars) as well as renilla luciferase driven by the CMV promoter (CMV-Luc, open bars). Representative data from three independent experiments done in triplicate are shown. Cells were transfected with 0.8 μg of HEXIM1-expressing plasmid for the indicated lanes, 0.1 μg of pCGtax for the indicated lanes, and 0.1 μg of pHTLV LTR Luc and 0.5 μg for phRL/CMV for all lanes. (d) The dose-dependent reduction of HIV-1 production by transfection of HEXIM1-encoding plasmids (0.1 μg for lanes 2 and 4, 0.4 μg for lanes 3 and 5) along with a plasmid producing infectious HIV-1 (pNL4-3, 0.1 μg) in HeLa-CD4 cells. (e–g) Expressing HEXIM1-f did not limit the replication of vaccinia virus (e), adenovirus (f), or HSV-1 (g) in 293T cells. The *y*-axis represents the reporter gene activity, which reflects viral replication. Representative data from three independent experiments are shown. GFP, green fluorescent protein; RLU, relative light unit.

could be readily identified by the green fluorescence. Human T cell lines, including SUP-T1, MOLT-4, CEM, Jurkat, and M8166 were infected with MLV pseudotyped with vesicular stomatitis virus glycoprotein (VSV-G), and GFP-positive cells were collected with a FACS (Fig. 2a). For the negative control, we used MLV expressing GFP only. The successful introduction of HEXIM1-f into the cells was verified by RT-PCR and Western blot analysis (Fig. 2b and c). The total HEXIM1 protein expression in HEXIM1-f-transduced cells was approximately 3.7-, 1.5-, 2.0-, 4.8-, and 1.8-fold higher than in GFP-transduced cells in the CEM, Jurkat, MOLT-4, SUP-T1, and M8166 cell lines, respectively (Fig. 2c). To our surprise, the HEXIM1-f-expressing T cell lines remained GFP-positive, and therefore HEXIM1-f-positive, for more than 6 months and proliferated at rates almost indistinguishable from GFP-expressing cells. The expression levels of cyclin T1, cyclin T2, actin, and Bip/GRK78 in HEXIM1-f-expressing cells were almost identical to those in GFP-expressing cells, suggesting that the gene expression did not compensate the upregulated HEXIM1 (Fig. 2b and c). Expression of cyclin T2 was undetectable in M8166 cells (Fig. 2c). Similarly, HEXIM1-f expression did not affect the cell surface levels of the HIV-1 receptors CD4 and CXCR4 as demonstrated by FACS analysis (data not shown). These data indicate that the expression of HEXIM1-f did not reach levels where the physiological regulation of P-TEFb blocked cellular gene transcription.

The replication kinetics of HIV-1 or SIV was monitored by measuring the accumulation of viral capsid antigen in the culture medium. Strikingly, HIV-1 replicated more slowly in cells of all four T cell lines expressing HEXIM1-f than in cells expressing GFP (Fig. 2d–g). Similarly, HEXIM1-f-expressing M8166 cells supported SIV replication less efficiently than did GFP-expressing M8166 cells (Fig. 2h). Interestingly, the magnitude of HIV-1 replication delay was the most substantial in SUP-T1 cells, in which the levels of endogenous HEXIM1 were the lowest among the four cell lines tested for HIV-1 replication (Fig. 2c). Similar observations were made when the HIV-1 infection experiments were repeated, indicating that the expression of functional HEXIM1-f did not change over the course of the replication monitoring. We tested whether the viruses emerged in

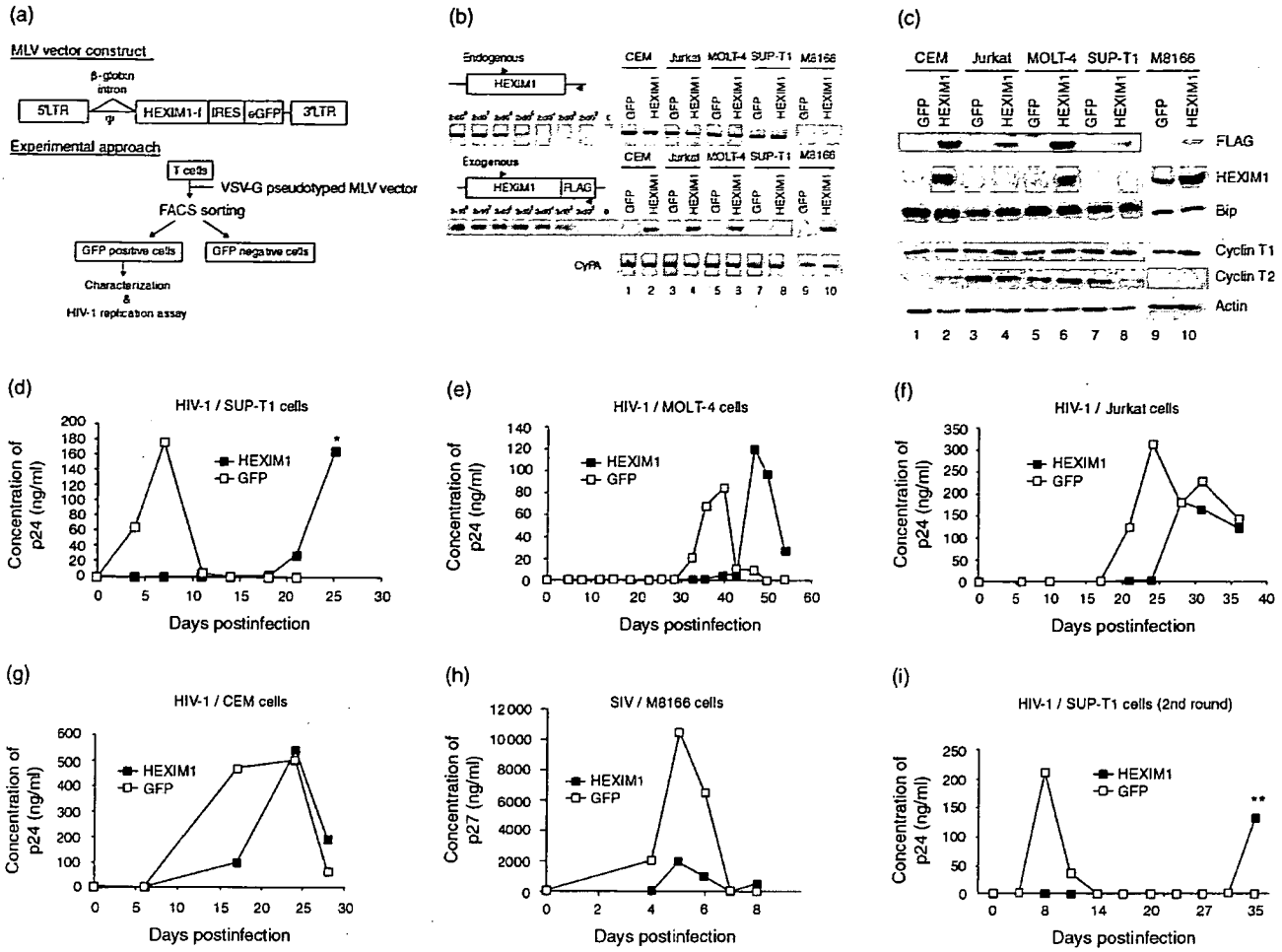

Fig. 2. Lentiviral replication is inhibited in various T cell lines constitutively expressing hexamethylene bisacetamide-induced protein 1 (HEXIM-1) cDNA tagged with a FLAG epitope at the carboxy terminus (HEXIM1-f). (a) The genomic organization of the retroviral vector expressing HEXIM1-f and a schematic representation of the experimental approach. (b) Detection of endogenous HEXIM1 and murine leukemia virus (MLV)-transduced HEXIM1-f (exogenous) mRNA by reverse transcriptase-polymerase chain reaction in green fluorescent protein (GFP)- and HEXIM1-f-expressing cells. The primer design is drawn schematically. Amplification efficiency was examined by using a known number of templates as standards for HEXIM1. Cyclophilin A (CyPA) was amplified to ensure the quality of the RNA. (c) Western blot analysis demonstrating expression of HEXIM1-f (denoted FLAG), endogenous HEXIM1 (HEXIM1), Bip, cyclin T1, cyclin T2, and actin in isolated T cell lines. (d–g) Replication profiles of HIV-1 (HXB2) in SUP-T1 (d), MOLT-4 (e), Jurkat (f), and CEM (g) cells either expressing HEXIM1-f or GFP alone. Representative data from two or three independent experiments are shown. (h) Replication profile of SIV in M8166 cells either expressing HEXIM1-f or GFP alone. Representative data from two independent experiments are shown. (i) The replication profiles of HIV-1 recovered from SUP-T1/HEXIM1-f cells (asterisk in Fig. 2d) in fresh SUP-T1/GFP or SUP-T1/HEXIM1-f. LTR, long terminal repeat.

HEXIM1-f-expressing cells were 'revertants' that might be able to replicate in HEXIM1-f-expressing cells as fast as in GFP-expressing cells. To address this, we recovered virus-containing culture supernatants from SUP-T1/HEXIM1-f cells at the peak of replication kinetics (asterisk, Fig. 2d). Then, both fresh SUP-T1/GFP and SUP-T1/HEXIM1-f were infected with the recovered virus and the replication kinetics was monitored. However, HIV-1 still replicated in SUP-T1/HEXIM1-f cells more slowly than in SUP-T1/GFP cells (Fig. 2i), akin to the original profiles (Fig. 2d), and the nucleotide sequences of LTR and *tat*, the primary targets of HEXIM1, remained unchanged (double asterisk in Fig. 2i). In addition, no mutations were found in viruses propagated in GFP-expressing SUP-T1 cells. Similar observations were made in MOLT-4 cells (data not shown). These data provide direct evidence that the expression of HEXIM1 inhibits lentiviral replication in human T cell lines.

Based on our experimental observations as well as the reported functions of HEXIM1, we assumed that the ability of HEXIM1 to limit HIV-1 replication was mostly due to the inhibition of Tat/P-TEFb-dependent transcriptional elongation. However, it was possible that HEXIM1 might also have targeted other viral replication

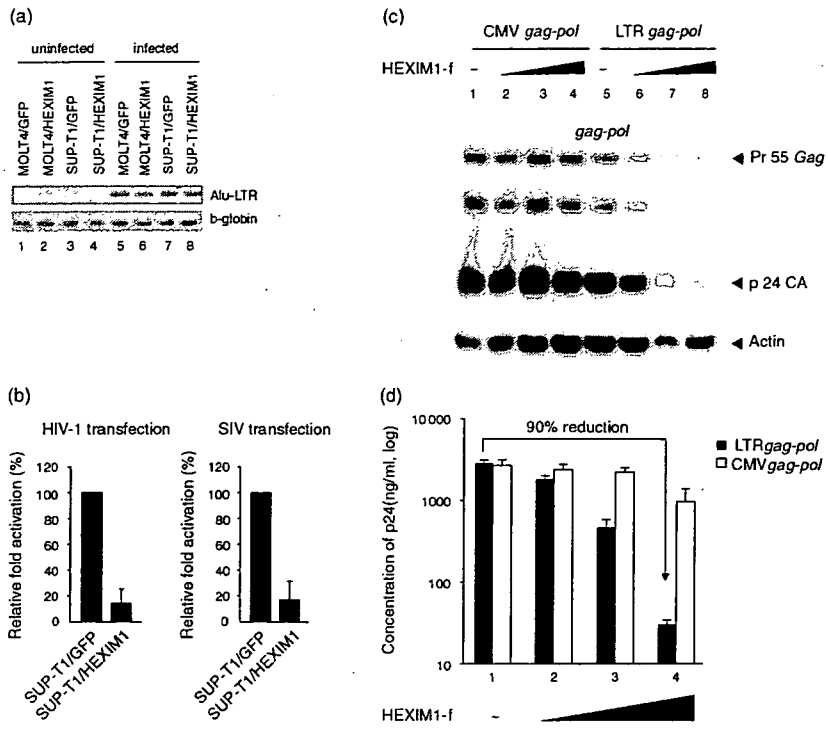

Fig. 3. Hexamethylene bisacetamide-induced protein 1 (HEXIM1) cDNA tagged with a FLAG epitope at the carboxy terminus (HEXIM1-f) does not affect the efficiency of viral integration or post-translational processes. (a) The Alu-long terminal repeat (LTR) and beta-globin polymerase chain reaction products from VSV-G-pseudotyped HIV-1-infected MOLT-4 and SUP-T1 cells expressing either green fluorescent protein (GFP) or HEXIM1-f alone were separated in an agarose gel and photographed. (b) The luciferase activities in SUP-T1/GFP or SUP-T1/HEXIM1-f cells electroporated with 10 μg of a plasmid encoding LTR-driven firefly luciferase plus 1 μg of phRL/cytomegalovirus (CMV). The firefly luciferase activity normalized to renilla luciferase activity in SUP-T1/GFP cells was set to 100%. The error bars represent the standard deviation of three independent experiments. (c) Western blot analysis showing Gag and its cleaved products expressed from either CMV promoter- or LTR promoter-driven *gag-pol* expression plasmid in the presence of pSVtat (0.1 μg, all lanes) and increasing amounts of HEXIM1-f (0.2 μg for lanes 2 and 6, 0.6 μg for lanes 3 and 7, and 2.0 μg for lanes 4 and 8). (d) The amount of p24 produced in the culture supernatant from cells analyzed in Fig. 3c was measured by enzyme-linked immunosorbent assay. Representative data from three independent experiments done in triplicate are shown. SIV, simian immunodeficiency virus.

steps. To test this possibility, we examined the viral entry and production processes separately. The efficiency of viral entry was analyzed by measuring the efficiency of viral integration. SUP-T1/GFP or SUP-T1/HEXIM1-f cells were infected with a replication-incompetent HIV-1 vector pseudotyped with VSV-G that expresses luciferase upon successful infection. We conducted an Alu-LTR PCR assay to detect the integrated viral genome. PCR products were detected only from HIV-1-infected cells (Fig. 3a). The signal intensities of Alu-LTR PCR products from GFP- and HEXIM1-f-experssing cells were similar. To compare the efficiency of viral infection as well as transcription quantitatively, we employed a real time PCR technique. Some infected cells were collected for an Alu-LTR PCR assay to quantify the amount of integrated viral genome, and the rest were processed to measure the amount of viral transcript as well as the luciferase activity. The amount of Alu-LTR PCR product from SUP-T1/HEXIM1-f cells was 3.5- and 3.3-fold more to that from SUP-T1/GFP cells from two independent experiments, respectively (Table 1). These data suggest that the efficiency of viral integration was not inhibited in HEXIM1-f-expressing SUP-T1 cells. In contrast, the relative abundance of HIV-1 transcript expressed in SUP-T1/HEXIM1-f cells was substantially decreased to 0.03 and 2.9% relative to SUPT1/GFP cells (Table 1). Furthermore, the luciferase activities were 200-fold lower in SUP-T1/HEXIM1-f cells than in SUP-T1/GFP cells (Table 1). Similar data was obtained from MOLT-4 cells infected with HIV-1 pseudotyped with VSV-G (data not shown). The transfection of plasmids encoding reporter viral DNA can bypass the viral entry and make it possible to measure the effect of HEXIM1 on LTR-driven transcription and translation. Consistent with above data, transfecting pNL-Luc into SUP-T1/HEXIM1-f cells gave significantly lower luciferase activities than SUP-T1/GFP cells (Fig. 3b, left). Similar data were obtained using pSIVmac239ΔnefLuc (Fig. 3b, right). These data strengthen the possibility that HEXIM1 targets post-integration processes.

Table 1. Effect of hexamethylene bisacetamide-induced protein 1 (HEXIM1) cDNA tagged with a FLAG epitope at the carboxy terminus (HEXIM1-f) on viral entry and transcription in SUP-T1 cells examined by quantitative real time polymerase chain reaction.

		Integrated HIV-1 genome			HIV-1 transcript			Luciferase activity	
Exp.	Transduced gene	Alu-LTR (copy)	β-globin (copy)	Normalized[a] (%)	HIV-1 RNA (copy)	CyPA (copy)	Normalized[b] (%)	RLU[c]	Normalized[d] (%)
1	GFP	5.2×10^5	6.7×10^6	100.0	1.6×10^6	6.8×10^7	100.0	3.2×10^5	100.0
	HEXIM1-f	2.0×10^6	7.4×10^6	351.3	6.7×10^1	1.0×10^8	0.03	1.5×10^3	0.5
2	GFP	4.6×10^6	1.8×10^7	100.0	3.1×10^8	8.9×10^7	100.0	7.1×10^5	100.0
	HEXIM1-f	1.6×10^7	1.9×10^7	333.2	9.4×10^6	9.3×10^7	2.9	3.4×10^3	0.5

[a]The number of Alu-long terminal repeat (LTR) products divided by the number of beta-globin products in SUP-T1/GFP is set to 100%. The abundance of Alu-LTR products in SUP-T1/HEXIM1-f relative to SUP-T1/green fluorescent protein (GFP) is shown.
[b]The number of HIV-1 RNA transcripts in SUP-T1/GFP divided by the number of cyclophilin A (CyPA) transcripts is set to 100%. The abundance of HIV-1 RNA in SUP-T1/HEXIM1-f relative to SUP-T1/GFP is shown.
[c]The luciferase activity is shown by relative light unit (RLU).
[d]The luciferase activity in SUP-T1/GFP is set to 100%. The luciferase activity in SUP-T1/HEXIM1-f relative to SUP-T1/GFP is shown.

To test this further, we analyzed the efficiency of post-transcriptional processes with a transient transfection assay measuring the amount of Pr55 Gag, a viral gene product, and virus-like particles (VLPs) produced in the culture supernatants. For this purpose, we used the CMV promoter-driven *gag-pol* expression plasmid, because HEXIM1-f did not affect CMV-driven transcription (Fig. 1b). At the levels of HEXIM1-f where LTR-driven Tat-dependent transcription was drastically inhibited (Fig. 3c, lanes 7, 8), the amount of CMV promoter-driven Gag expression was almost identical to that in the absence of HEXIM1-f (Fig. 3c, lanes 1–4). Furthermore, the processing pattern of Pr55 Gag in the presence of HEXIM1-f was identical to that in its absence (Fig. 3c). These data indicate that HEXIM1-f did not inhibit the transcription from a Tat-independent promoter, the translation of viral protein, or the protease activity of HIV-1. Finally, the potential effect of HEXIM1 on viral budding was examined. To do this, the amount of p24 CA in the culture supernatant of transfected cells was quantified as a representation of the amount of VLP. Expressing HEXIM1-f reduced VLP production from cells co-transfected with pLTR*gag-pol* and pSVtat at levels comparable to the protein expression levels (Fig. 3c and d). In contrast, expressing HEXIM1-f did not reduce the amount of VLP produced by cells co-transfected with pCMV*gag-pol* and pSVtat in conditions in which Tat-dependent LTR transcription was substantially inhibited (Fig. 3c and d). Taken together, this indicates that HEXIM1-f lowers the efficiency of Tat-dependent transcription from LTR promoter but does not block the efficiency of the late phase of the viral life cycle including translation, Gag's assembly, and budding. Thus, it is likely that HEXIM1 primarily targets Tat/P-TEFb-dependent transcription to inhibit HIV-1 replication.

Our findings demonstrated that HEXIM1, a cellular P-TEFb inhibitor, is a specific negative regulator of lentiviral replication in human T cell lines. The replication of vaccinia virus, adenovirus, and HSV-1 were not affected by HEXIM1-f expression; however, the *Tat*-dependent transcription of the LTR promoter of both HIV-1 and SIV was reduced by HEXIM1-f. HEXIM1 limited replication of HIV-1 dramatically at levels where it did not visibly affect cell physiology (as little as a 5-fold increase over the endogenous levels), nor were revertants immediately selected in HEXIM1-f-expressing cells. These data support the feasibility of developing HIV-1 inhibitors targeting the processes in which HEXIM1 is involved. For example, it is conceivable to hunt for a non-toxic chemical inducer for HEXIM1 since expression of HEXIM1 is induced by hexamethylene bisacetamide (HMBA) that is considerably toxic for cells [20].

P-TEFb has been shown to support transcription of the *c-myc* and CIITA transcription factors (reviewed in [21,22]). The functions of these transactivators are critical for cell proliferation, but in this study constitutive expression of HEXIM1-f, which reduces P-TEFb activity, did not affect the cell proliferation of human T cell lines, the human epithelial cell lines HEK293 or the NP2 glioblastoma cell lines (data not shown). How can this be explained? Very recently, a high-molecular-weight bromodomain protein, Brd4, was found to function as a 'cellular *tat*' [23,24]. Interestingly, it was shown that Brd4 binds not only to cyclin T1 but also to cyclin T2, a widely expressed variant of cyclin T, to which HEXIM1 binds but Tat does not [23–25]. We hypothesize that Brd4 might be able to recruit and activate P-TEFb more efficiently than does Tat, leaving cellular transcription unaffected by the upregulated expression of HEXIM1 from the retroviral vector. An alternative possibility comes from the fact that HEXIM1 does not interact with the ubiquitously expressed cyclin K, which functions as a P-TEFb component. It is possible that Tat is not able to utilize P-TEFb consisting of CDK9 and cyclin K but Brd4 can, such that cyclin K may substitute for cyclin T1 to support Brd4-mediated cellular gene transcription.

Acknowledgements

We thank Dr. Tsutomu Murakami for the critical reading of the manuscript. This work was partly supported by

Japan Health Science Foundation, Japanese Ministry of Health, Labor and Welfare, and Japanese Ministry of Education, Culture, Sports, Science and Technology.

Sponsorship: This work was partly supported by Japan Health Science Foundation, Japanese Ministry of Health, Labor and Welfare, and Japanese Ministry of Education, Culture, Sports, Science and Technology.

References

1. Marshall N, Price D. **Control of formation of two distinct classes of RNA polymerase II elongation complexes.** *Mol Cell Biol* 1992; **12**:2078–2090.
2. Kuiken C, Foley B, Hahn B, Korber B, Marx P, McCutchan F, *et al.*, editors. *HIV Sequence Compendium 2000.* Los Alamos: Theoretical Biology and Biophysics Group, Los Alamos National Laboratory, 2000.
3. Barboric M, Peterlin BM. **A new paradigm in eukaryotic biology: HIV Tat and the control of transcriptional elongation.** *PLoS Biol* 2005; **3**:e76.
4. Nguyen V, Kiss T, Michels A, Bensaude O. **7SK small nuclear RNA binds to and inhibits the activity of CDK9/cyclin T complexes.** *Nature* 2001; **414**:322–325.
5. Yang Z, Zhu Q, Luo K, Zhou Q. **The 7SK small nuclear RNA inhibits the CDK9/cyclin T1 kinase to control transcription.** *Nature* 2001; **414**:317–322.
6. Li Q, Price J, Byers S, Cheng D, Peng J, Price D. **Analysis of the large inactive P-TEFb complex indicates that it contains one 7SK molecule, a dimer of HEXIM1 or HEXIM2, and two P-TEFb molecules containing Cdk9 phosphorylated at threonine 186.** *J Biol Chem* 2005; **280**:28819–28826.
7. Michels A, Nguyen V, Fraldi A, Labas V, Edwards M, Bonnet F, *et al.* **MAQ1 and 7SK RNA interact with CDK9/cyclin T complexes in a transcription-dependent manner.** *Mol Cell Biol* 2003; **23**:4859–4869.
8. Yik J, Chen R, Pezda A, Samford C, Zhou Q. **A human immunodeficiency virus type 1 Tat-like arginine-rich RNA-binding domain is essential for HEXIM1 to inhibit RNA polymerase II transcription through 7SK snRNA-mediated inactivation of P-TEFb.** *Mol Cell Biol* 2004; **24**:5094–5105.
9. Barboric M, Kohoutek J, Price J, Blazek D, Price D, Peterlin B. **Interplay between 7SK snRNA and oppositely charged regions in HEXIM1 direct the inhibition of P-TEFb.** *EMBO J* 2005; **24**:4291–4303.
10. Schulte A, Czudnochowski N, Barboric M, Schonichen A, Blazek D, Peterlin B, Geyer M. **Identification of a cyclin T-binding domain in Hexim1 and biochemical analysis of its binding competition with HIV-1 Tat.** *J Biol Chem* 2005; **280**:24968–24977.
11. Fraldi A, Varrone F, Napolitano G, Michels A, Majello B, Bensaude O, Lania L. **Inhibition of Tat activity by the HEXIM1 protein.** *Retrovirology* 2005; **2**:42.
12. Michels A, Fraldi A, Li Q, Adamson T, Bonnet F, Nguyen V, *et al.* **Binding of the 7SK snRNA turns the HEXIM1 protein into a P-TEFb (CDK9/cyclin T) inhibitor.** *EMBO J* 2004; **23**:2608–2619.
13. Komano J, Miyauchi K, Matsuda Z, Yamamoto N. **Inhibiting the Arp2/3 complex limits infection of both intracellular mature vaccinia virus and primate lentiviruses.** *Mol Biol Cell* 2004; **15**:5197–5207.
14. Wagner R, Graf M, Bieler K, Wolf H, Grunwald T, Foley P, Uberla K. **Rev-independent expression of synthetic gag-pol genes of human immunodeficiency virus type 1 and simian immunodeficiency virus: implications for the safety of lentiviral vectors.** *Hum Gene Ther* 2000; **11**:2403–2413.
15. Masuda T, Planelles V, Krogstad P, Chen I. **Genetic analysis of human immunodeficiency virus type 1 integrase and the U3 att site: unusual phenotype of mutants in the zinc finger-like domain.** *J Virol* 1995; **69**:6687–6696.
16. Willey R, Smith D, Lasky L, Theodore T, Earl P, Moss B, *et al.* **In vitro mutagenesis identifies a region within the envelope gene of the human immunodeficiency virus that is critical for infectivity.** *J Virol* 1988; **62**:139–147.
17. Butler SL, Hansen MS, Bushman FD. **A quantitative assay for HIV DNA integration in vivo.** *Nat Med* 2001; **7**:631–634.
18. Graf Einsiedel H, Taube T, Hartmann R, Wellmann S, Seifert G, Henze G, Seeger K. **Deletion analysis of p16(INKa) and p15(INKb) in relapsed childhood acute lymphoblastic leukemia.** *Blood* 2002; **99**:4629–4631.
19. Zhou M, Lu H, Park H, Wilson-Chiru J, Linton R, Brady JN. **Tax interacts with P-TEFb in a novel manner to stimulate human T-lymphotropic virus type 1 transcription.** *J Virol* 2006; **80**: 4781–4791.
20. Kusuhara M, Nagasaki K, Kimura K, Maass N, Manabe T, Ishikawa S, *et al.* **Cloning of hexamethylene-bis-acetamide-inducible transcript, HEXIM1, in human vascular smooth muscle cells.** *Biomed Res* 1999; **20**:273–279.
21. Price DH. **P-TEFb, a cyclin-dependent kinase controlling elongation by RNA polymerase II.** *Mol Cell Biol* 2000; **20**:2629–2634.
22. Garriga J, Grana X. **Cellular control of gene expression by T-type cyclin/CDK9 complexes.** *Gene* 2004; **337**:15–23.
23. Jang M, Mochizuki K, Zhou M, Jeong H, Brady J, Ozato K. **The bromodomain protein Brd4 is a positive regulatory component of P-TEFb and stimulates RNA polymerase II-dependent transcription.** *Mol Cell* 2005; **19**:523–534.
24. Yang Z, Yik J, Chen R, He N, Jang M, Ozato K, Zhou Q. **Recruitment of P-TEFb for stimulation of transcriptional elongation by the bromodomain protein Brd4.** *Mol Cell* 2005; **19**:535–545.
25. Napolitano G, Licciardo P, Gallo P, Majello B, Giordano A, Lania L. **The CDK9-associated cyclins T1 and T2 exert opposite effects on HIV-1 Tat activity.** *AIDS* 1999; **13**:1453–1459.

THE JOURNAL OF BIOLOGICAL CHEMISTRY VOL. 282, NO. 50, pp. 36671–36681, December 14, 2007

A Suppressive Role of the Prolyl Isomerase Pin1 in Cellular Apoptosis Mediated by the Death-associated Protein Daxx*

Received for publication, May 21, 2007, and in revised form, September 17, 2007 Published, JBC Papers in Press, October 15, 2007, DOI 10.1074/jbc.M704145200

Akihide Ryo[‡1], Akiko Hirai[‡], Mayuko Nishi[‡], Yih-Cherng Liou[§2], Kilian Perrem[¶], Sheng-Cai Lin[‖], Hisashi Hirano[**], Sam W. Lee[‡‡], and Ichiro Aoki[‡]

From the [‡]Department of Pathology, Yokohama City University School of Medicine, 3-9 Fuku-ura, Kanazawa-ku, Yokohama 236-0004, Japan, the [§]Department of Biological Sciences, National University of Singapore, Singapore 117543, Singapore, the [¶]Molecular Oncology Laboratory, Department of Pathology, Royal College of Surgeons in Ireland, Smurfit Building, Beaumont Hospital, Dublin 9, Ireland, the [‖]Key Laboratory of the Ministry of Education for Cell Biology, School of Life Sciences, Xiamen University, Fujian 361005, Xiamen, China, the [**]International Graduate School of Arts and Sciences, Yokohama City University, Yokohama 230-0045, Japan, and the [‡‡]Cutaneous Biology Research Center, Massachusetts General Hospital and Harvard Medical School, Charlestown, Massachusetts 02129

The death-associated protein Daxx is a multifunctional factor that regulates a variety of cellular processes, including transcription and apoptosis. Several previous reports have indicated that Daxx is induced upon oxidative stress and is then subjected to phosphorylation-based functional modification. However, the precise molecular events underlying these phosphorylation events remain largely unknown. We report in our current study that the peptidyl-prolyl isomerase Pin1 is highly overexpressed in malignant human gliomas and inhibits Daxx-mediated cellular apoptosis. The targeted inhibition of Pin1 by small interfering RNA in A172 glioblastoma cells significantly enhances the apoptotic response induced by hydrogen peroxide or stimulatory Fas antibodies. This is in turn accompanied by the increased induction of Daxx and the activation of the apoptosis signal-regulating kinase 1/c-Jun N-terminal kinase pathway. Furthermore, Pin1 binds to the phosphorylated Ser^{178}-Pro motif in the Daxx protein, and Pin1 overexpression results in the rapid degradation of Daxx via the ubiquitin-proteasome pathway. Moreover, a Daxx-S178A mutant, which cannot interact with Pin1, demonstrates higher proapoptotic activity and is refractory to Pin1-mediated antiapoptotic effects. We further found that the expression levels of Pin1 inversely correlate with the degree of Daxx nuclear accumulation in human glioblastoma tissues. These results together indicate that Pin1-mediated prolyl isomerization plays an important role in the negative regulation of Daxx and thereby inhibits the oxidative stress-induced cellular apoptotic response, particularly in malignant tumor cells where Pin1 is often overexpressed.

Oncogenesis comprises a complex series of multistep and multifactorial processes that result in uncontrolled cell proliferation, cell transformation, and cell death (1). The resistance to apoptosis in malignant tumor cells is one of the most critical factors that directly contribute to tumor cell proliferation and expansion (2). Furthermore, this apoptotic evasion represents one of the true hallmarks of cancer and appears to be a vital component in chemotherapeutic and radiotherapeutic resistance that characterizes the aggressiveness of human malignant tumors (1).

The antiapoptotic characteristics of tumor cells are often derived from the improper regulation of proapoptotic signaling pathways by various external and internal stimuli (3). One of the pivotal signaling mechanisms that controls cellular apoptotic processes is the phosphorylation of proteins on serine or threonine residues preceding proline (Ser/Thr-Pro) (4, 5). The recent identification and characterization of the peptidyl-prolyl isomerase Pin1, which can recognize these phosphorylated moieties, has led to the elucidation of a number of novel postphosphorylation regulatory mechanisms (4). Pin1 catalyzes the cis-trans isomerization of phosphorylated Ser/Thr-Pro motifs within its specific target substrates (4, 5). Pin1-mediated prolyl isomerization has also now been shown to function in several signaling pathways during tumorigenesis, including Wnt/β-catenin and NF-κB (6, 7). Pin1 is further implicated in many pivotal oncogenic cellular events, such as cell proliferation, angiogenesis, and tumor metastasis (8). However, although some of the roles of Pin1 in several oncogenic signaling pathways have been addressed, there has been no direct evidence reported to date showing that Pin1 can inhibit cellular apoptosis in malignant tumor cells.

The death-associated protein Daxx was originally identified as a Fas-interacting protein that specifically binds to the death domain of Fas and then facilitates Fas-mediated apoptosis independently of FADD (9). Several lines of evidence presented in recent studies have indicated that Daxx plays a crucial role in the cellular apoptotic response induced by UV, oxidative stress, and glucose deprivation, in addition to its function during Fas-mediated apoptosis (10). Daxx has also been reported to localize at the promyelocytic leukemia nuclear bodies in nonapoptotic cells (11). Indeed, nuclear Daxx has been demonstrated to regulate transcription by acting as a transcriptional corepressor via its interaction with several transcription factors (12). Several additional studies have also addressed the potential cyto-

* This work was supported in part by a special fellow grant from the Leukemia and Lymphoma Society and by grants from the Ministry of Education, Culture, Sports, Science and Technology of Japan (to A. R.). The costs of publication of this article were defrayed in part by the payment of page charges. This article must therefore be hereby marked "*advertisement*" in accordance with 18 U.S.C. Section 1734 solely to indicate this fact.

[1] To whom correspondence should be addressed. Tel.: 81-45-787-2587; Fax: 81-45-786-0191; E-mail: aryo@yokohama-cu.ac.jp.

[2] Supported by grants from the National Science Foundation of China and the Biomedical Research Council of Singapore.

plasmic *versus* nuclear roles of Daxx toward the triggering of apoptotic pathways (13). Upon various stimuli, such as serum depletion or oxidative stress, Daxx is phosphorylated and retranslocated from the cytoplasm to the nucleus via the exportin-mediated nuclear transport system (14). Cytoplasmic Daxx can interact with apoptosis signal-regulating kinase 1 (ASK1)[3] and then activate the ASK1/c-Jun-N-terminal kinase (JNK) signaling pathway. In fact, Daxx-depleted cells have been shown to be resistant to cell death pathways induced by both UV irradiation and oxidative stress following impaired ASK1/JNK activation (13). Although the phosphorylation of Daxx has also been shown to regulate its subcellular localization and function following proapoptotic stimuli, it is not known whether its protein stability is regulated by phosphorylation or by other post-translational modifications.

The aim of our present study was to clarify the regulation of Daxx by phosphorylation-dependent prolyl isomerization mediated by Pin1. The importance of both the physical and functional interactions between Daxx and Pin1 during the induction of cell death pathways following exposure to oxidative stress was also investigated, and the involvement of the ASK1/JNK pathway was also evaluated. We find from the results of these analyses that the targeted inhibition of Pin1 in human glioblastoma A172 cells significantly sensitizes these cells to oxidative stress-induced apoptosis, suggesting that Pin1 can protect against the Daxx-mediated apoptotic response. We also find that Pin1 can bind Daxx via its phosphorylated Ser^{178}-Pro motif and facilitate its prompt degradation via the ubiquitin-proteasome pathway. This results in the inhibition of the proapoptotic functions of Daxx. Our present results have thus uncovered a novel molecular mechanism underlying the post-translational regulation of Daxx and demonstrate that Pin1 acts as a putative antiapoptotic molecule in malignant tumor cells.

EXPERIMENTAL PROCEDURES

Immunohistochemistry—Human glioma tissue microarrays (US Biomax, Rockville, MD) were analyzed immunohistochemically using a Pin1 antibody as previously described (15). Briefly, paraffin-embedded tissue sections were deparaffinized and rehydrated. After microwave antigen retrieval in sodium citrate buffer, endogenous peroxidase activity was quenched by immersion in 0.3% H_2O_2. The sections were then treated with anti-Pin1 polyclonal antibodies (Santa Cruz Biotechnology, Santa Cruz, CA) at a 1:200 dilution overnight at 4 °C, after blocking with 5% normal goat serum for 30 min at room temperature. Biotinylated goat anti-rabbit immunoglobulin G (Vector Laboratories, Burlingame, CA) was then used as the secondary antibody at a 1:200 dilution for 30 min at room temperature. The sections were subsequently treated using a peroxidase-labeled Vectastain Elite ABC kit (Vector Laboratories), at a 1:200 dilution for 30 min at room temperature. Labeled antigen was visualized via a 3,3′-diaminobenzidine reaction, and each of the sections was counterstained with hematoxylin. The expression level of Pin1 was evaluated as described previously (15).

Retroviral siRNA Infection—A Pin1-specific siRNA retroviral vector was prepared as previously described (8). Target cell lines were treated with the indicated retrovirus and selected by continuous growth in puromycin (1.0–1.5 μg/ml) for 48 h to isolate stable clones.

siRNA Oligonucleotides—Human Daxx siRNA and scrambled control siRNA oligonucleotides were purchased from Santa Cruz Biotechnology. The final concentration of siRNA oligonucleotides was 200 nmol/liter, and these molecules were introduced into cells using Lipofectamine 2000 (Invitrogen) according to the manufacturer's instructions.

Cell Culture and Transient Transfections—A172, 293T, and HeLa cells were cultured in Dulbecco's modified Eagle's medium supplemented with 10% fetal bovine serum and 1% penicillin (100 mg/ml), streptomycin (50 μg/ml). Transient transfections were carried out using either Effectene Transfection Reagent (Qiagen) or HilyMax (DOJINDO, Kumamoto, Japan).

Protein Degradation Assay—Protein degradation assays were performed as described previously (6). Briefly, 293T cells were co-transfected with FLAG-Daxx and either wild-type Pin1 or empty vector, with GFP used as a transfection control. Cycloheximide (50 μg/ml) was added to the medium 24 h after transfection, and the cells were harvested at different time points. Total cell lysates in SDS sample buffer were boiled and then analyzed by immunoblotting with either anti-FLAG (Sigma) or anti-Pin1 (R&D System) or GFP (Invitrogen) antibodies.

GST Pull-down, Immunoprecipitation, and Immunoblotting Analyses—293T cells was lysed with GST pull-down buffer (50 mM HEPES (pH 7.4), 150 mM NaCl, 10% glycerol, 1% Triton X-100, 1.5 mM $MgCl_2$, 1 mM EGTA, 1 mM EDTA, 100 mM NaF, 1 mM Na_3VO_4, 1 mM dithiothreitol, 0.5 μg/ml leupeptin, 1.0 μg/ml pepstatin, 10 μM MG132, 10 μM MG115, and 0.2 mM phenylmethylsulfonyl fluoride) and incubated with 30 μl of glutathione-agarose beads containing either GST-Pin1 or GST at 4 °C for 2 h. The precipitated proteins were then washed three times with GST pull-down buffer and subjected to SDS-PAGE (7). For immunoprecipitation, cells were harvested 24 h after transfection and lysed with radioimmune precipitation buffer (20 mM Tris-HCl (pH 7.5), 150 mM NaCl, 2 mM EDTA, 1% Nonidet P-40, 1% sodium deoxycholate, 0.1% SDS, 1 mM Na_3VO_4, 50 mM NaF, 0.5 μg/ml leupeptin, 1.0 μg/ml pepstatin, 10 μM MG132, 10 μM MG115, and 0.2 mM phenylmethylsulfonyl fluoride). Cell lysates were then incubated for 1 h with protein A/G-Sepharose-nonimmunized IgG complexes. Supernatant fractions were recovered and immunoprecipitated with 5 μg of anti-FLAG or anti-Myc antibody and 30 μl of protein A/G-Sepharose. After washing three times with radioimmune precipitation buffer, pellets were analyzed on SDS-polyacrylamide gels and subjected to immunoblotting analysis. The antibodies used in this study were obtained from the following sources: mouse monoclonal anti-Daxx, mouse monoclonal anti-Fas (SH-11), and rabbit polyclonal anti-GFP antibodies (MBL International); rabbit polyclonal anti-phospho-ASK1 (Ser^{83}) and cleaved caspase-3 (Asp^{175}) antibodies (Cell Signal-

[3] The abbreviations used are: ASK1, apoptosis signal-regulating kinase 1; TUNEL, terminal deoxynucleotidyltransferase-mediated deoxyuridine triphosphate biotin nick end labeling; JNK, c-Jun N-terminal kinase; siRNA, small interfering RNA; GFP, green fluorescent protein; GST, glutathione S-transferase; PPIase, prolyl isomerase.

ing); mouse monoclonal anti-phospho-JNK (Thr(P)[183]/Tyr(P)[185]) antibody (BD Biosciences); rabbit polyclonal anti-Pin1 (H-123) and rabbit polyclonal anti-JNK (C-17) antibodies (Santa Cruz Biotechnology); anti-Pin1 monoclonal antibody (R & D Systems); rabbit polyclonal anti-cleaved poly(ADP-ribose) polymerase antibody (Abcam); mouse monoclonal anti-FLAG (M2); and anti-γ-tubulin antibodies (Sigma).

Fluorescence Imaging—HeLa cells on coverslips were co-transfected with pDs-Red-Daxx and pIRES-puro-GFP-Pin1 using HilyMax (DOJINDO), according to the manufacturer's instructions. 24 h after transfection, the cells were fixed with 3% formaldehyde and treated with phosphate-buffered saline and were then stained with 4′, 6-diamidino-2-phenylindole. After washing with phosphate-buffered saline, slides were visualized under a confocal laser microscope (Olympus, Tokyo, Japan) as described previously (16).

Apoptosis Analysis—Apoptotic cells were detected by the *in situ* TUNEL method using a DeadEnd Colorimetric TUNEL system (Promega), according to the manufacturer's protocol. Cells with apoptotic nuclei were detected by Hoechst 33258 staining with fluorescent microscopy as described previously (17). Cell viability was investigated with a trypan blue dye exclusion assay using 0.4% trypan blue dye (Sigma). The data were expressed as the mean ± S.D. from triplicate independent experiments.

In Vitro Kinase Assay—For the measurement of JNK1 activity *in vitro*, A172 cells were lysed in buffer containing 25 mM HEPES (pH 7.4), 150 mM NaCl, 20 mM β-glycerophosphate, 2 mM EDTA, 2 mM EGTA, 50 mM NaF, 1 mM sodium orthovanadate, 1% Triton X-100, and proteinase inhibitor mixture, as described previously (18). The lysates were then clarified by centrifugation and immunoprecipitated with the anti-JNK antibody C-17 (Santa Cruz Biotechnology) for 2 h. The immune complexes were recovered with protein A-Sepharose beads and washed twice with the above lysis buffer and twice with kinase buffer (25 mM HEPES (pH 7.4), 20 mM $MgCl_2$, 20 mM β-glycerophosphate, 0.5 mM EGTA, 0.5 mM NaF, 0.5 mM sodium orthovanadate). The immune complexes on the Sepharose beads were used in kinase assays with GST-c-Jun. The reaction was initiated by adding 30 μl of kinase reaction mixture (kinase buffer plus 5 μCi of [γ-^{32}P]ATP, 20 μM unlabeled ATP, 1 mM dithiothreitol, and 1 μg of a substrate). After 20 min of incubation at 30 °C, the reactions were terminated by the addition of 10 μl of 5× SDS-PAGE loading buffer. Samples were resolved by SDS-PAGE and visualized by autoradiography.

RESULTS

Pin1 Is Highly Expressed in Human Glioma—It has been previously reported that Pin1 is highly overexpressed in various human malignancies, including breast and prostate cancers, and plays a crucial role in oncogenesis (4, 5). Since the relevance of Pin1 in the tumorigenesis of human glioma has not been well characterized, we investigated the correlation of Pin1 expression with the malignant properties of human gliomas. To this end, we first performed immunohistochemical analysis of a human glioma tissue panel, including normal brain tissue controls (n = 9), low grade astrocytomas (grade 2; n = 24), anaplastic astrocytomas (grade 3; n = 45), and glioblastomas (grade 4; n = 28), all classified according to World Health Organization criteria. We found that Pin1 expression was significantly enhanced in glioma tissues compared with normal brain (Fig. 1*A*). Interestingly, Pin1 expression was found to be confined to the nuclei in both normal brain tissue and low grade astrocytoma at relatively low expression levels but exhibited enhanced expression in both the cytoplasm and nuclei of anaplastic astrocytoma and glioblastoma (Fig. 1*A*), as previously found also in other malignant tumors (15, 19). These immunohistochemical analyses indicate that the higher expression of Pin1 correlates with a more highly malignant glioma (Fig. 1*B*). Our results thus suggest a potential role for Pin1 in the development of these tumors.

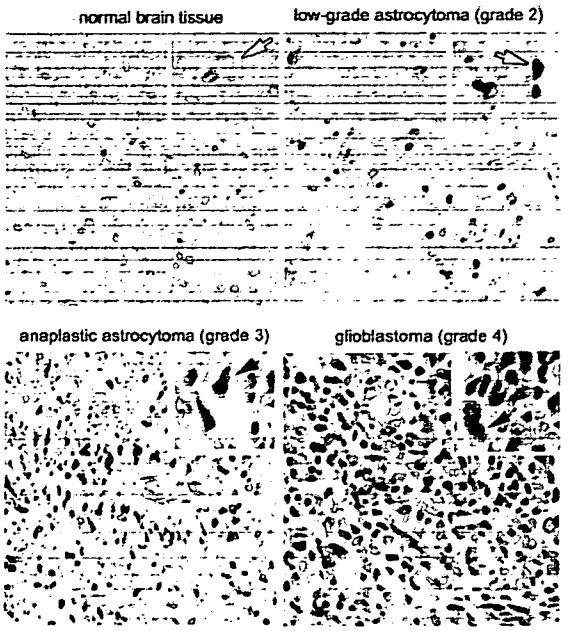

B

Pin1 expression	Low level	High level	Very high level	Total
Normal brain	9(100%)	0(0%)	0(0%)	9(100%)
Grade2	4(16.7%)	13(54.2%)	7(29.2%)	24(100%)
Grade3	3(6.7%)	20(44.4%)	22(35.7%)	45(100%)
Grade4	3(10.7%)	15(53.6%)	10(35.7%)	28(100%)
Total	19(17.9%)	48(45.3%)	39(36.8%)	106(100%)

FIGURE 1. **Pin1 is overexpressed in human glioma tissues.** *A*, tissues, including normal brain, a low grade astrocytoma (grade 2), an anaplastic astrocytoma (grade 3), and a glioblastoma (grade 4), were immunostained with anti-Pin1 antibodies. Nuclei were further stained with hematoxylin. Pin1 signals in nuclei only and in both the nuclei and cytoplasm are indicated by the *white* and *black arrows*, respectively. *B*, the ratio of cells with low, high, or very high Pin1 expression levels was scored for each of the glioma tissues in a panel of different grades and also in normal brain. A significant correlation between Pin1 expression levels and glioma grades was confirmed using a Spearman rank test ($p < 0.01$).

Loss of Pin1 Function Sensitizes Human Glioblastoma Cells to Oxidative Stress-induced Cell Death—Our immunohistochemical analysis suggested that high levels of Pin1 expression in human gliomas could contribute to the acquisition of some of the malignant characteristics of these tumors. It has been reported that high grade gliomas are resistant to cellular apoptosis and that this could be important for tumor cell proliferation and drug resistance (20). To investigate whether Pin1 contributes to apoptotic resistance in glioma cells, we attempted to create stable human glioma cell lines in which Pin1 is constitutively suppressed.

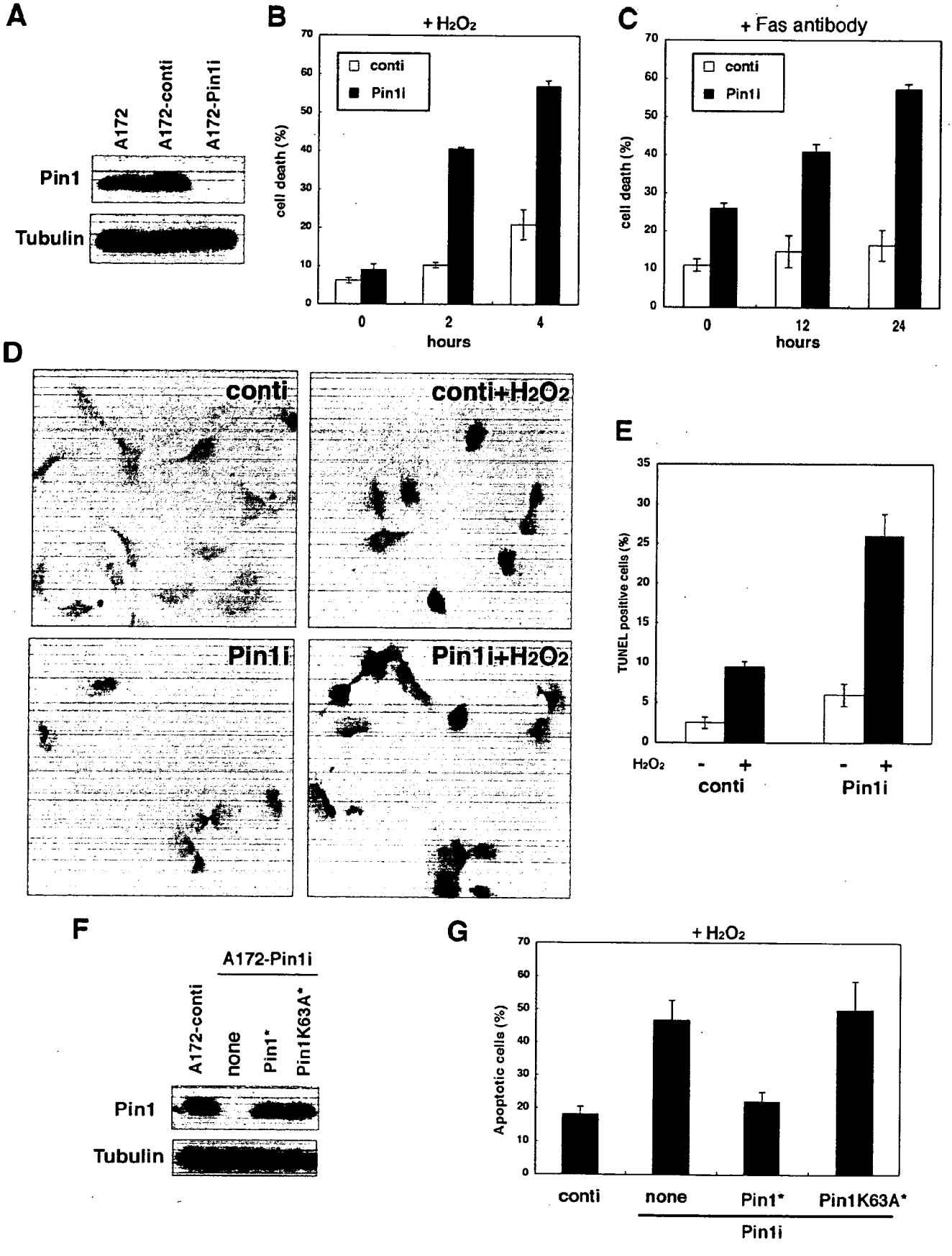

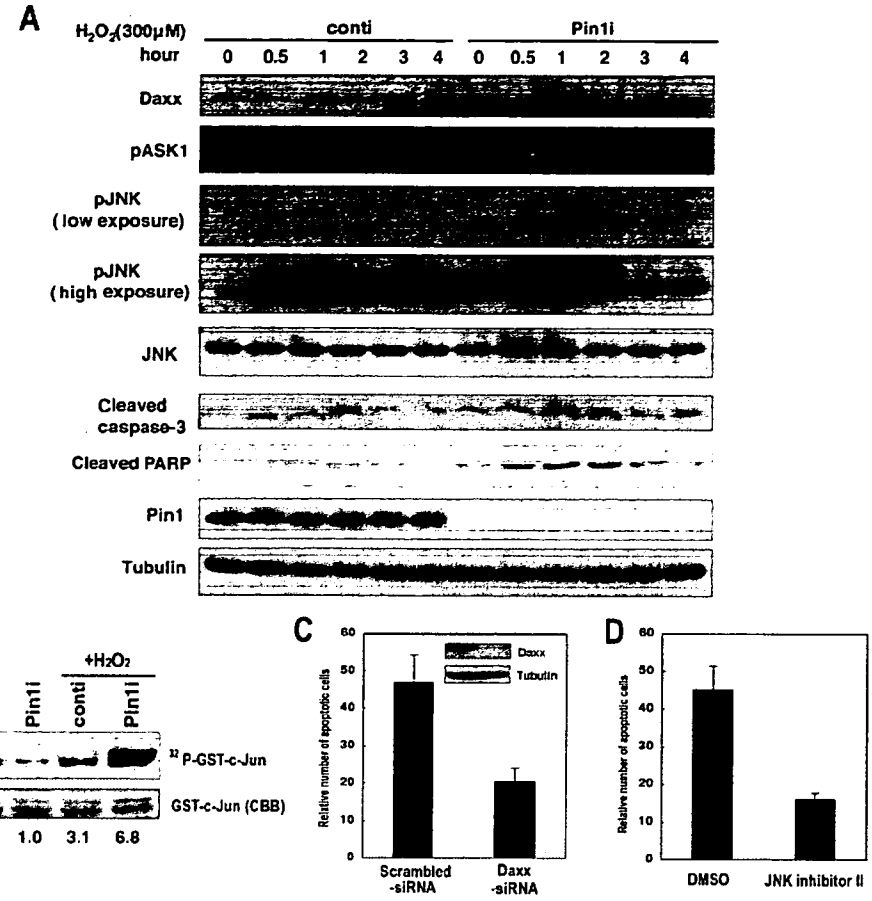

FIGURE 3. **The stable suppression of Pin1 enhances H_2O_2-induced Daxx expression and ASK1/JNK activation under conditions of oxidative stress.** *A*, A172 stable cells were treated with H_2O_2 (300 μM) and harvested at the indicated time points followed by immunoblotting with the indicated antibodies. *B*, A172 stable cells were untreated or treated with H_2O_2 (300 μM). After 3 h, cells were harvested and subjected to immunoprecipitation with anti-JNK1 antibody followed by *in vitro* kinase assay using GST-c-Jun as a substrate. *Numbers below* the *blots* indicate band intensity of ^{32}P-labeled c-Jun quantitated by a PhosphorImager. *CBB*, Coomassie Brilliant Blue stain. *C*, A172-Pin1-siRNA (Pin1i) stable cells were transfected with either nonspecific (*scrambled*) or Daxx-targeted siRNA oligonucleotides. At 36 h after transfection, the cells were treated with H_2O_2 (300 μM) for 4 h and stained with Hoechst 33258 dye. Relative apoptotic cell numbers were scored out of 200 cells. *Inset*, immunoblotting with the indicated antibodies. *D*, A172-Pin1-siRNA (Pin1i) stable cells were pretreated with either JNK inhibitor II (20 μM) or Me_2SO for 1 h and then exposed to H_2O_2 (300 μM) for another 4 h. The relative numbers of apoptotic cell were scored as in *C*. *DMSO*, Me_2SO.

To this end, we employed a representative human glioblastoma cell line, A172, since these cells have been reported to show antiapoptotic properties against oxidative stress stimuli and anti-tumor drugs (21). The retrovirus-mediated siRNA targeting of Pin1 in A172 cells (A172-Pin1i) was found to cause a marked knockdown of Pin1 expression (<95%), whereas the control siRNA expressing cells (A172-conti) showed Pin1 expression levels that were similar to the noninfected cells (Fig. 2*A*). We next treated these stable cell lines with either hydrogen peroxide (H_2O_2) or anti-Fas stimulatory antibodies to induce cellular apoptosis. We found that Pin1 depletion by siRNA significantly enhances the rate of cell death caused by both of these stimuli by ~3-fold compared with the control siRNA-expressing cells (Fig. 2, *B* and *C*). Consistent with these results, the A172-Pin1i cells exhibit a higher rate of TUNEL staining compared with A172-conti cells when treated with H_2O_2 (Fig. 2, *D* and *E*). Furthermore, the forced expression of wild-type Pin1, but not its peptidyl-prolyl isomerase mutant (K63A), which was not subject to knockdown by siRNA, reverted the apoptotic response in cells harboring Pin1 siRNA molecules to control levels (Fig. 2, *F* and *G*). These results verify that there is a specific role of endogenous Pin1 in the suppression of H_2O_2- or Fas-induced cellular apoptosis and suggest that the targeted inhibition of Pin1 in glioma cells causes an increased susceptibility to cellular apoptosis induced by oxidative stress.

The Suppression of Pin1 Enhances Daxx Induction and Subsequent ASK1/JNK Activation toward Oxidative Stress-induced Cellular Apoptosis—Our initial analysis indicated that the specific depletion of Pin1 enhances the apoptotic response to oxidative stress in human glioma cells. To delineate the molecular events underlying this phenomenon, we performed immunoblotting analysis to monitor the activity of the intracellular signaling pathways related to oxidative stress-induced cellular apoptosis. Since it has been reported that the activation of the Daxx-ASK1-JNK pathway is a critical event in the induction of cellular apoptosis by H_2O_2 (3), we evaluated the components of this pathway in our current experiments.

FIGURE 2. **The loss of Pin1 function sensitizes human glioblastoma cells to oxidative stress-induced cellular apoptosis.** *A*, stable suppression of Pin1 by retrovirus-mediated siRNA in A172 glioblastoma cells determined by immunoblotting analysis. Lysates from cells that were mock-infected or retrovirally infected with control siRNA (*conti*) or Pin1-specific siRNA (*Pin1i*) were immunoblotted with either anti-Pin1 or anti-γ-tubulin antibodies. *B* and *C*, the stable siRNA cell lines described in *A* were treated with either H_2O_2 (300 μM) (*B*) or stimulatory Fas antibodies (100 ng/ml) (*C*). At the indicated time points following these treatments, viable cell numbers were counted using trypan blue dye exclusion (mean ± S.D.). *D* and *E*, A172 stable cell lines treated with H_2O_2 (300 μM) were subjected to TUNEL staining. TUNEL-positive cells were visualized by staining with diaminobenzene (*DAB*; *brown*). Cells were also counterstained with 1% methyl green (*green*). TUNEL-positive cells were scored out of >200 cells from three independent experiments. *F* and *G*, A172-Pin1i cells were transfected with siRNA-resistant wild type Pin1 (*Pin1**) or a PPIase domain mutant Pin1-K63A (*Pin1-K63A**) and co-transfected with GFP as a transfection control. The expression of these Pin1 constructs was initially confirmed by immunoblot analysis with anti-Pin1 antibody (*F*). After 24 h, cells were seeded onto glass coverslips and treated with H_2O_2 (300 μM) for another 4 h. Cells were then fixed and immunostained with anti-cleaved caspase-3 antibody. The ratios of cleaved caspase-3-positive cells to GFP-positive cells were calculated from three independent experiments (mean ± S.D.) (*G*).

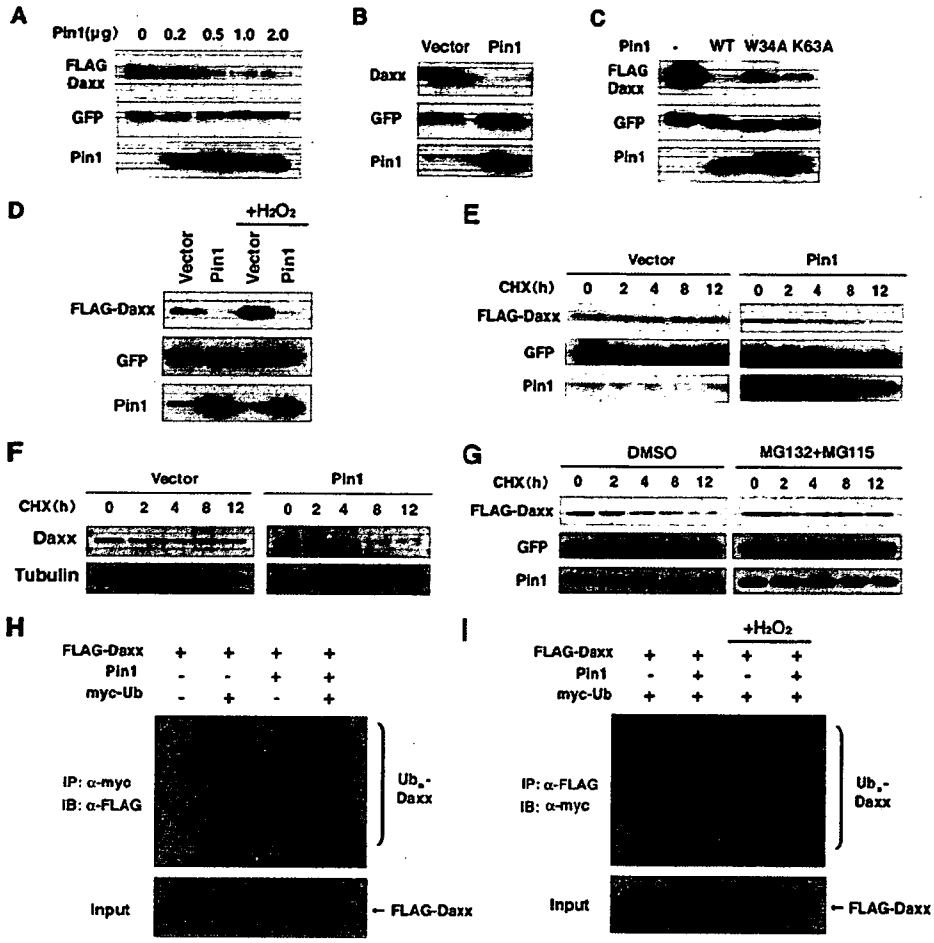

FIGURE 4. **Pin1 expression facilitates the degradation of Daxx via the ubiquitin-proteasome pathway.** *A*, 293T cells were co-transfected with FLAG-Daxx, GFP, or different amounts of Pin1 expression plasmids. After 24 h, the cells were harvested and subjected to immunoblotting analysis with either anti-FLAG or anti-GFP antibodies. *B*, 293T cells were transfected with either wild-type Pin1 or empty vector. After 24 h, the cells were subjected to immunoblotting with an anti-Daxx antibody to monitor the endogenous Daxx levels. *C*, 293T cells were transfected with FLAG-Daxx and co-transfected with either wild-type Pin1 (*WT*) or its W34A (WW domain) or K63A (PPIase domain) mutants. After 24 h, the cells were subjected to immunoblotting as indicated. *D*, 293T cells were co-transfected with FLAG-Daxx and GFP and co-transfected with either wild-type Pin1 or empty vector. After 24 h, the cells were treated with H_2O_2 for 3 h and then subjected to immunoblotting as indicated. *E*, 293T cells were co-transfected with the indicated vectors, treated with cycloheximide (*CHX*) after 24 h, and harvested at the indicated time points. This was followed by immunoblotting analysis with either anti-FLAG or anti-GFP antibodies. *F*, 293T cells were transfected with either Pin1 or control vector subjected to a cycloheximide assay as shown in *E*. Cells were harvested at the indicated time points followed by immunoblotting analysis. *G*, 293T cells were subjected to a cycloheximide assay, as shown in *E*, in the presence or absence of the proteasome inhibitors MG132 and MG115 (10 μM each). *H*, 293T cells were co-transfected with the indicated vectors and cotreated with the proteasome inhibitors MG132 and MG115 after 24 h. After a further 12 h, the cell lysates were subjected to immunoprecipitation (*IP*) analysis with anti-Myc antibodies followed by immunoblotting (*IB*) with anti-FLAG antibodies. Ub_n, polyubiquitinated. *I*, 293T cells were co-transfected with the indicated vectors. After 24 h following transfection, cells were treated with the proteasome inhibitor MG132 and MG115 (10 μM each) with or without H_2O_2 for 5 h. The cell lysates were subjected to immunoprecipitation analysis with anti-FLAG antibodies followed by immunoblotting with anti-Myc antibodies. Ub_n, polyubiquitinated; *DMSO*, Me_2SO.

A172-Pin1i cells demonstrate a more prominent induction of the Daxx protein upon H_2O_2 treatment, compared with control cells (Fig. 3*A*). Following this enhanced Daxx induction, the phosphorylation of both ASK1 and JNK, indicating activation, was consistently increased in A172-Pin1i cells compared with control cells (Fig. 3*A*). Furthermore, the levels of cleaved caspase-3 and cleaved PARP, indicating apoptosis, were observed to be significantly higher in Pin1-depleted cells (Fig. 3*A*), consistent with data from our TUNEL analysis (Fig. 2*D*). An *in vitro* kinase assay further demonstrated that JNK activity was significantly increased in A172-Pin1i cells following H_2O_2 treatment when compared with the control cells (Fig. 3*B*). These results indicate that the inhibition of Pin1 may sensitize the cells to the apoptotic response induced by H_2O_2 by augmenting the induction and activation of the Daxx-ASK1-JNK pathway. To confirm this possibility, we transduced Daxx-specific siRNA oligonucleotides to block endogenous Daxx expression as well as treated the cells in parallel experiments with the JNK inhibitor II (SP600125). We found that either Daxx siRNA or SP600125 treatment could significantly reduce the susceptibility of A172-Pin1i cells to H_2O_2-induced cellular apoptosis (Fig. 3, *C* and *D*). This indicates that the targeted depletion of Pin1 enhances the induction of Daxx, thereby augmenting the apoptotic response via the ASK1/JNK pathway upon oxidative stress.

Pin1 Facilitates the Degradation of Daxx via the Ubiquitin-Proteasome Pathway—Since the depletion of Pin1 was found to enhance the expression of Daxx following oxidative stress, we speculated whether the corollary would be true, such that high levels of Pin1 might in fact inhibit the expression of Daxx. To test this possibility, we initially co-transfected A172 cells with FLAG-tagged Daxx and Pin1 and then examined the expression levels of Daxx. Immunoblotting analysis demonstrated that Pin1 reduces the exogenously transduced FLAG-Daxx levels in a dose-dependent manner (Fig. 4*A*). Moreover, the expression levels of endogenous Daxx were also found to be reduced in these Pin1-overexpressed cells (Fig. 4*B*). Interestingly, the mRNA levels of Daxx are not altered upon Pin1 overexpression (data not shown), indicating that Pin1 might affect the protein stability of Daxx.

To address whether either the binding or the catalytic activity of Pin1 is required for the suppression of Daxx, we performed a parallel experiment using either a WW domain (binding domain) mutant (W34A) or PPIase domain (catalytic domain) mutant (K63A) of Pin1. Neither of these mutants fully down-regulate FLAG-Daxx expression (Fig. 4*C*), indicating that both the WW and PPIase domains are indeed required for this function of Pin1.

We next performed parallel experiments with or without H_2O_2 treatment. Pin1 overexpression was found to suppress Daxx expression in both untreated and H_2O_2-treated cells (Fig. 4*D*), indicating that Pin1 affects Daxx expression independently of H_2O_2 exposure.

Cycloheximide analysis also revealed that the protein stability of both endogenously and exogenously expressed Daxx is significantly reduced when Pin1 is overexpressed (Fig. 4, *E* and *F*), further indicating that Pin1 enhances the degradation of Daxx. To address whether this is mediated by the ubiquitin-proteasome pathway, we performed parallel experiments using the proteasome inhibitors MG132 and MG115. Treatment with these inhibitors significantly inhibited the degradation of Daxx following Pin1 overexpression (Fig. 4*G*). Moreover, immunoprecipitation analysis with cells co-transfected with FLAG-Daxx and Myc-ubiquitin, with or without Pin1 co-transfection, further revealed that Pin1 overexpression significantly enhances the polyubiquitination of the Daxx protein (Fig. 4*H*). Furthermore, the reciprocal ubiquitination analysis with or without H_2O_2 treatment further revealed that Pin1 enhances the polyubiquitination of Daxx irrespective of H_2O_2 exposure (Fig. 4*I*). These results together confirm that Pin1 enhances the degradation of the Daxx protein via the ubiquitin-proteasome pathway independently of proapoptotic stimuli, such as H_2O_2 treatment.

Pin1 Interacts with Daxx Phosphorylated on Its Ser^{178}-Pro Motif—Our previous results indicated that Pin1 could affect the protein stability of Daxx by mediating the ubiquitination status of this protein. We next examined whether Pin1 could directly interact with Daxx. Immunoprecipitation analysis revealed that this is indeed the case (Fig. 5*A*). GST pull-down analyses further demonstrated that wild-type Pin1 binds the Daxx protein but that the Pin1 WW domain mutant W34A does not (Fig. 5*B*). The association between Pin1 and Daxx was also found to be completely abolished by pretreatment of the cell lysates with calf intestine alkaline phosphatase prior to the GST pull-down analysis (Fig. 5*C*), indicating that Pin1 binds only phosphorylated Daxx. Interestingly, the interaction between Pin1 and Daxx could be observed in both the absence and the presence of H_2O_2 stimulation (Fig. 5*B*), indicating that this interaction is independent of the corresponding stress response and that the Pin1 binding motif in Daxx may be constitutively phosphorylated in these cells.

Immunofluorescence analysis further demonstrated that Pin1 co-localizes with Daxx in intranuclear aggregates corresponding to promyelocytic leukemia bodies in the absence of H_2O_2 stimulation, as reported previously (11) (Fig. 5*D*). Upon H_2O_2 stimulation, certain subsets of both Daxx and Pin1 were found to translocate diffusely into the cytoplasm, although the majority of these proteins were still retained in the nucleus and colocalized together in nuclear bodies (Fig. 5*D*).

To identify the specific Pin1 binding site in the Daxx protein, we created several Daxx deletion mutants and performed GST pull-down analysis. These experiments revealed that an N-terminal Daxx deletion mutant (Δ1–36) could still bind Pin1 but also that an extended N-terminal deletion mutant (Δ1–183) failed to do so (Fig. 6*A*). These data indicate that Pin1 binds to Daxx in the region between amino acids 36 and 183.

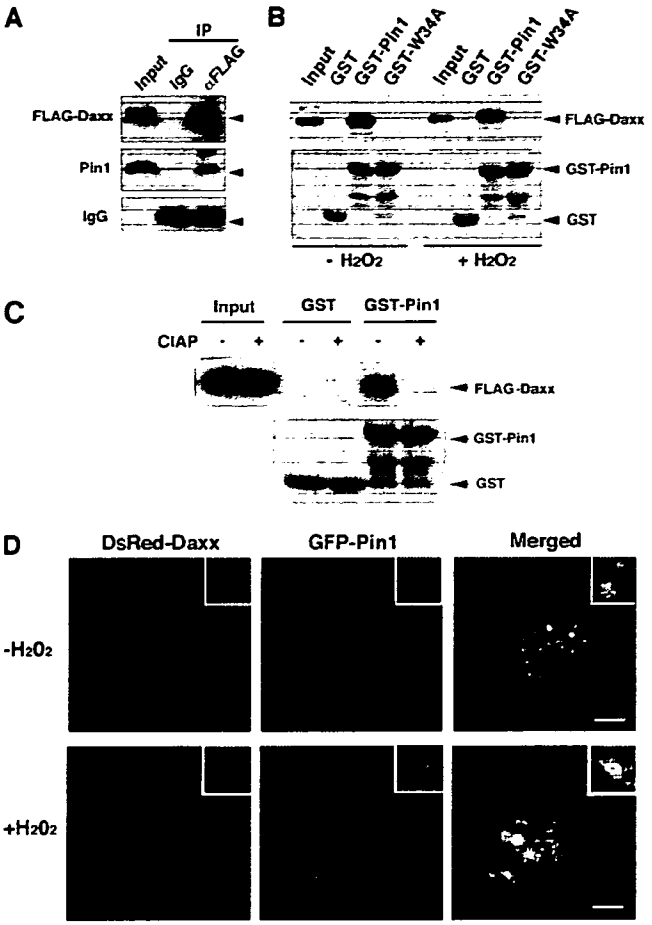

FIGURE 5. **Pin1 interacts with phosphorylated Daxx.** *A*, 293T cells were transfected with FLAG-Daxx and Pin1. After 24 h, cell lysates were subjected to immunoprecipitation (*IP*) analysis with anti-FLAG or nonimmunized IgG followed by immunoblotting analysis with anti-FLAG or anti-Pin1 antibodies. *B*, 293T cells were transfected with FLAG-Daxx. After 24 h, cell lysates were subjected to GST pull-down analysis with GST, GST-Pin1, or GST-Pin1W34A mutant followed by immunoblotting with anti-FLAG antibody. *C*, cell lysates derived from 293T cells transfected with FLAG-Daxx were treated or untreated with calf intestine alkaline phosphatase (*CIAP*), followed by GST pull-down analysis as described in *B*. *D*, HeLa cells were co-transfected with GFP-Pin1 and Ds-Red-Daxx. After 24 h, the cells were treated or untreated with H_2O_2 for 3 h. Cells were then fixed and stained with 4′,6-diamino-2-phenylindole (*DAPI*) and then subjected to confocal microscopy. *Scale bar*, 10 μm.

Previous reports have indicated that Pin1 can bind only phosphorylated Ser/Thr-Pro motifs (4, 5). Since there is only a single Ser/Thr-Pro motif (Ser^{178}-Pro) between residues 36 and 183 in the Daxx protein, we created a Daxx site-directed mutant at this site by substituting the serine 178 with alanine (S178A). Moreover, we created an additional Daxx mutant by substitution of serine 668 with alanine (S668A), since this site has been shown to be phosphorylated (14). Both GST pull-down and immunoprecipitation analyses subsequently revealed that Pin1 binds both wild-type and the S668A mutant Daxx proteins but not the S178A mutant (Fig. 6, *B* and *C*). These results confirm that Pin1 indeed binds the phosphorylated Ser^{178}-Pro motif of Daxx.

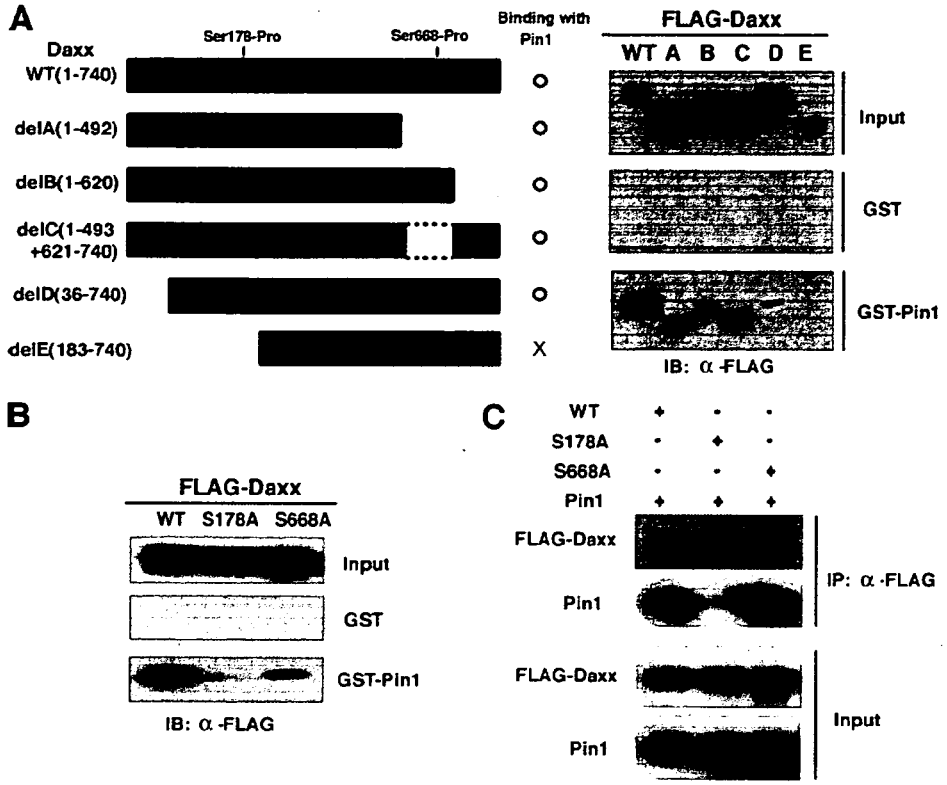

FIGURE 6. **Pin1 interacts with Daxx via its Ser^{178}-Pro motif.** *A (left)*, schematic representation of the Daxx deletion mutants generated in this study. *Right*, 293T cells were transfected with the indicated Daxx-deletion mutants for 24 h. Cell lysates were then subjected to GST pull-down followed by immunoblotting analysis. *B*, 293T cells were transfected with the indicated Daxx site-directed mutants and subjected to GST pull-down analysis as shown in *A*. *C*, 293T cells were co-transfected with the indicated Daxx constructs. At 24 h following transfection, the cells were treated with the proteasome inhibitors MG132 and MG115 (10 μM each). After 12 h, cell lysates were harvested and subjected to immunoprecipitation analysis with anti-FLAG antibodies followed by immunoblotting analysis with the indicated antibodies. *WT*, wild type.

The Daxx-S178A Mutant Is Refractory to Pin1-mediated Degradation and Shows Strong Proapoptotic Properties—To further examine the functional interactions between Pin1 and Daxx, we initially investigated the nature of the S178A mutant in terms of its protein stability. Cycloheximide analysis revealed that the S178A Daxx mutant is resistant to degradation following the co-transfection of Pin1 (Fig. 7*A*). Consistent with this result, this S178A mutant also shows lower levels of ubiquitination compared with wild-type Daxx upon Pin1 co-transfection (Fig. 7*B*). A reciprocal immunoprecipitation analysis further revealed that the S178A mutant was refractory to be polyubiquitinated following Pin1 overexpression as compared with wild-type Daxx (Fig. 7*C*). These results together confirm that the direct interaction between Pin1 and Daxx via the Ser^{178}-Pro motif augments the ubiquitination of Daxx and thereby enhances its degradation by the proteasome.

We next examined the proapoptotic properties of the S178A Daxx mutant in the absence or presence of exogenous Pin1. A previous report has indicated that the co-transfection of Daxx and its downstream target ASK1 initiates apoptosis in HeLa cells (22). We therefore co- transfected HeLa cells with ASK1 and either FLAG-Daxx or S178A Daxx in the presence or absence of Pin1. As shown in Fig. 7, *D* and *E*, the co-transfection of ASK1 with either wild-type or S178A mutant Daxx results in cellular apoptosis. However, the S178A mutant shows stronger proapoptotic effects compared with wild type Daxx. Furthermore, when co-transfected with Pin1, the S178A mutant still retains its potent ability to induce cellular apoptosis, which is in contrast to wild-type Daxx, which fails to induce apoptosis in the presence of high levels of Pin1, as revealed by either immunostaining for cleaved caspase-3 or Hoechst 33258 staining for apoptotic nuclei (Fig. 7, *D* and *E*). These results together indicate that the proapoptotic properties of the S178A mutant are refractory to the antiapoptotic function of Pin1.

Reverse Correlation between Pin1 and Daxx Expression in Human Glioblastoma Tissues—To further examine the pathological role of Pin1 in the degradation of Daxx, we determined the expression levels of the Daxx protein in the 28 grade 4 human glioblastoma tissues that we analyzed earlier for Pin1 expression by immunohistochemical staining. As shown in Fig. 1, Pin1 is expressed to various degrees in human glioblastoma tissues. Consistent with our molecular data, we found that Daxx staining was predominantly absent in glioma tissues containing high levels of Pin1 and that Daxx accumulation in the nucleus was evident in cases containing relatively low expression levels of Pin1 (Fig. 8*A*). Among the 28 grade 4 human glioblastoma tissues that we examined, there was also a significant reverse correlation between Pin1 expression and the immunoreactivity of Daxx, as determined by the Spearman rank correlation test ($p < 0.01$) (Fig. 8*B*). These results further support the notion that Pin1 is important for the regulation of Daxx expression *in vivo* and strengthen the significance of Pin1 overexpression in the negative regulation of Daxx in malignant human glioma.

DISCUSSION

In our current study, we report that the peptidyl-prolyl isomerase Pin1 associates with phosphorylated Daxx and enhances its degradation, resulting in the prevention of oxidative stress-induced cellular apoptosis. We find that 1) Pin is highly overexpressed in human gliomas, and its expression levels parallel the malignant properties of the glioma cells; 2) Pin1-depleted A172 glioblastoma cells are highly susceptible to cellular apoptosis induced by either hydrogen peroxide or stimulatory Fas antibodies; 3) Pin1 inhibition enhances the induction of Daxx and the activation of the ASK1/JNK apoptotic pathway; 4) Pin1 overexpression causes the rapid degradation of the Daxx protein via the ubiquitin-proteasome pathway; 5) Pin1 interacts with Daxx via its phosphorylated Ser^{178}-Pro

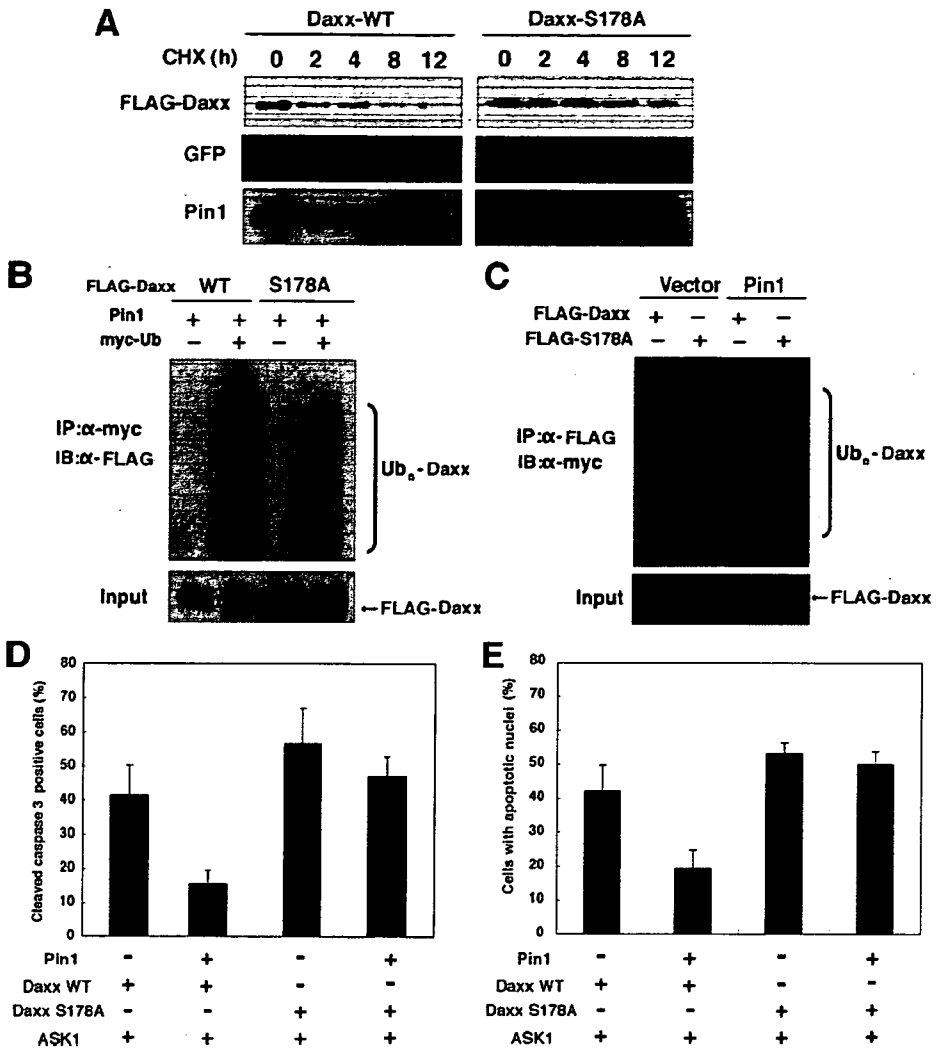

FIGURE 7. **The Daxx-S178A mutant is refractory to Pin1-mediated degradation and shows strong pro-apoptotic properties in the presence of Pin1.** *A*, 293T cells were co-transfected with the indicated constructs. After 24 h, cells were treated with CHX and harvested at the indicated time points followed by immunoblotting analysis. *B*, 293T cells were co-transfected with the indicated vectors. At 24 h following transfection, the cells were treated with the proteasome inhibitors MG132 and MG115 (10 μM each). After 12 h, cell lysates were harvested and subjected to immunoprecipitation (*IP*) analysis with anti-Myc antibodies followed by immunoblotting (*IB*) with anti-FLAG antibodies. *C*, 293T cells were co-transfected with the indicated vectors. At 24 h following transfection, the cells were treated with the proteasome inhibitors MG132 and MG115 (10 μM each). After 12 h, cell lysates were harvested and subjected to immunoprecipitation analysis with anti-FLAG antibodies followed by immunoblotting with anti-Myc antibodies. *D* and *E*, HeLa cells were co-transfected with ASK1 and either wild-type Daxx or its S178A mutant and co-transfected with either GFP or GFP-Pin1. After 30 h, the cells were fixed and subjected to immunofluorescent analysis with anti-cleaved caspase-3 antibodies followed by the Hoechst 33258 staining. The relative apoptotic cell numbers are scored by counting 200 GFP-positive cells with either caspase-3-positive (*D*) or apoptotic (*E*) nuclei by Hoechst 33258 staining. *WT*, wild type.

evade programmed cell death (1). One of the current major issues in the clinical treatment of human glioma is the resistance of many of these tumors to chemotherapy (2). In our current report, however, we show that Pin1 inhibition increases the sensitivity of glioma cells to both H_2O_2 and Fas-mediated apoptosis and that this is accompanied by the increased expression of Daxx. In contrast, Pin1 overexpression significantly suppresses the expression of Daxx, thereby enhancing its degradation via the ubiquitin-proteasome pathway. These data suggest that aberrantly high levels of Pin1 in tumor cells can contribute to a blockade of proapoptotic pathways and promote the inappropriate survival of tumor cells. The inhibition of Pin1 may therefore be an effective strategy for the future treatment of glioma.

The involvement of Pin1 in cellular apoptosis has been addressed previously. First, Pin1 has been shown to interact with both p53 and p73, thereby affecting their stability. This modifies both the cell cycle-regulatory mechanisms and apoptotic pathways induced by genotoxic stress stimuli (23–25). Second, Pin1 also binds the antiapoptotic protein Bcl-2 during mitosis at a proline-rich loop region, thereby blocking its cytoprotective and ion channel-forming activities (26). Pin1 has also been reported to interact with the BH3-only protein BIMEL, thus inducing apoptosis in neurons (27). These results indicate multiple effects of Pin1 on cellular apoptosis in different tissues or cell types via its interaction with specific substrate proteins. However, given that the Daxx-ASK1-JNK pathway plays a crucial role in cellular apoptosis by various proapoptotic stimuli and that this signaling pathway is often deregulated in many human tumors (10), our current study uncovers an important molecular mechanism by which malignant tumor cells with aberrantly high Pin1 levels could evade Daxx-mediated apoptosis. This in turn could directly contribute to tumor expansion and resistance to anticancer therapies.

It has been suggested that the subcellular localization of Daxx might determine its activity and function toward the induction of proapoptotic signaling, and this is critically regulated by multiple related factors. Several lines of evidence have now indi-

motif, and the Daxx-S178A mutant is refractory to both Pin1-mediated degradation and the anti-apoptotic effects of Pin1; and 6) there is a significant reverse correlation between the expression of Pin1 and Daxx in human glioblastoma tissues. These results are the first to demonstrate that Pin1-mediated prolyl isomerization plays a crucial role in the post-translational regulation of Daxx. Furthermore, we have shown that Pin1 significantly suppresses the Daxx-mediated apoptotic response in human glioma cells as a potent antiapoptosis factor.

Cancer cells often exhibit several types of malignant behavior, including a self-sufficiency in terms of growth signals, insensitivity to growth-inhibitory signals, and the ability to